Organic Process Research & Development **2006**, *10,* 628–643

Analysis of Two-Liquid-Phase Multistep Biooxidation Based on a Process Model: Indications for Biological Energy Shortage

Bruno Bühler,[†] Adrie J. J. Straathof,[‡] Bernard Witholt,[§] and Andreas Schmid*[,†]

Chair of Chemical Biotechnology, University of Dortmund, D-44221 Dortmund, Germany, Department of Biotechnology, Delft University of Technology, Julianalaan 67, NL-2628 BC Delft, The Netherlands, and Institute of Biotechnology, ETH Zurich, CH-8093 Zurich, Switzerland

Abstract:

A process model for whole-cell biocatalysis in a two-liquid-phase system including cell growth and bioconversion kinetics was developed. The reaction considered is the kinetically controlled multistep oxidation of pseudocumene to 3,4-dimethylbenzaldehyde catalyzed by recombinant *Escherichia coli* expressing the *Pseudomonas putida* genes encoding xylene monooxygenase (XMO). XMO catalyzes the successive oxygenation of one methyl group of xylenes to corresponding alcohols, aldehydes, and acids. The biocatalytic process includes cells growing in fed-batch mode and a two-liquid-phase system consisting of bis-(2-ethylhexyl)phthalate as organic carrier solvent and an aqueous minimal medium in a phase ratio of 1:1. The process model comprises a description of the bioconversion kinetics, mass transfer kinetics, cell growth, and mass balances for both the aqueous and the organic phase. Bioconversion kinetics and consistent process simulation indicated the occurrence of direct substrate uptake from the organic phase and provided evidence for a pH-influenced competition for NADH between XMO and the respiratory chain with its consequential impact on bioconversion and cell growth. For the simulation of such differential NADH limitation, a pH-dependent feedback inhibition of the NADH consuming bioconversions was introduced as a modeling tool, which allowed good simulations of biotransformation experiments performed at varying pH, scale, and initial substrate concentration. Moreover, modeling indicated a product inhibition in the second oxidation step, which could be confirmed experimentally. A sensitivity analysis for the aqueous−organic mass transfer coefficient showed that this transfer is not critical for the process performance and emphasized the efficient substrate-cell transfer in the investigated two-liquid-phase process. Based on a process model, this study provides an in-depth analysis of a biooxidation process based on growing cells with indications for biological energy shortage as a limiting factor.

1. Introduction

Regio- and stereospecific oxidations are an important field in biocatalysis.[1−4] Such reactions are often cofactor dependent (e.g., NADH, NADPH) and catalyzed by multicomponent enzyme systems, of which some are membrane associated. Thus, living whole-cells are usually favored over the use of isolated enzymes. Such potential preparative in vivo applications are often hampered by low water solubilities and high toxicities of substrates and products, limiting the performance of aqueous systems. Nonconventional reaction media such as an aqueous−organic two-liquid-phase system are promising alternatives.[5,6] A second, water-immiscible phase can act as a reservoir for substrate and products, regulating the concentration of such compounds in the biocatalyst microenvironment, minimizing toxicity, and simplifying product recovery.[7−10]

Here, we focus on a two-liquid-phase process for the production of aromatic aldehydes, which serve as ingredients of natural flavors and fragrances and as synthons for a variety of polymers, pharmaceuticals, and fine chemicals.[11,12] Synthetic chemical strategies such as carbonylation or oxygen addition usually require the use of expensive and hazardous reactants and catalysts and often yield product mixtures complicating product isolation.[13−15] Thus, we consider it worth exploring the biocatalytic production of aromatic aldehydes via selective multistep biooxidation of cheap substrates such as xylenes using the two-liquid-phase concept as a tool to control multistep whole-cell biocatalysis.

* To whom correspondence should be addressed: Chair of Chemical Biotechnology, Department of Biochemical & Chemical Engineering, University of Dortmund, Emil Figge Str. 66, D-44221 Dortmund, Germany. Telephone: +49 231 755 7380. Fax: +49 231 755 7382. E-mail: schmid@bci.uni-dortmund.de.

[†] University of Dortmund.

[‡] Delft University of Technology.

[§] ETH Zurich.

(1) Faber, K. *Biotransformations in Organic Chemistry*, 4th ed.; Springer: Berlin, Germany, 2000.
(2) Schmid, A.; Dordick, J. S.; Hauer, B.; Kiener, A.; Wubbolts, M.; Witholt, B. *Nature* **2001**, *409*, 258−268.
(3) Burton, S. G.; Cowan, D. A.; Woodley, J. M. *Nat. Biotechnol.* **2002**, *20*, 37−45.
(4) Schmid, A.; Hollmann, F.; Park, J. B.; Bühler, B. *Curr. Opin. Biotechnol.* **2002**, *13*, 359−366.
(5) de Smet, M.-J.; Wynberg, H.; Witholt, B. *Appl. Environ. Microbiol.* **1981**, *42*, 811−816.
(6) Schwartz, R. D.; McCoy, J. *Appl. Environ. Microbiol.* **1977**, *34*, 47−49.
(7) Woodley, J. M.; Lilly, M. D. *Chem. Eng. Sci.* **1990**, *45*, 2391−2396.
(8) Witholt, B.; Favre-Bulle, O.; Lageveen, R.; Kingma, J.; van Beilen, J. B.; Marvin, H.; Preusting, H. In *Pseudomonas: Molecular Biology and Biotechnology*; Galli, E., Silver, S., Witholt, B., Eds.; ASM Press: Washington, DC, 1992; pp 301−314.
(9) Salter, G. J.; Kell, D. B. *Crit. Rev. Biotechnol.* **1995**, *15*, 139−177.
(10) Leon, R.; Fernandes, P.; Pinheiro, H. M.; Cabral, J. M. S. *Enzyme Microb. Technol.* **1998**, *23*, 483−500.
(11) Bruehne, F.; Wright, E. In *Ullmann's Encyclopedia of Industrial Chemistry*; Gerhartz, W., Ed.; Wiley-VHC: Weinheim, Germany, 1985; Vol. A3, pp 463−474.
(12) Falbe, J.; Regitz, M. *CD Roempp Chemie Lexikon*, Version 1.0; Georg Thieme Verlag: Stuttgart, Germany, 1995.
(13) Carelli, I.; Chiarotto, I.; Cacchi, S.; Pace, P.; Amatore, C.; Jutand, A.; Meyer, G. *Eur. J. Org. Chem.* **1999**, 1471−1473.
(14) Thomas, J. M.; Raja, R.; Sankar, G.; Bell, R. G. *Nature* **1999**, *398*, 227−230.
(15) Labinger, J. A.; Bercaw, J. E. *Nature* **2002**, *417*, 507−514.

Published on Web 04/25/2006

10.1021/op060028g CCC: $33.50 © 2006 American Chemical Society

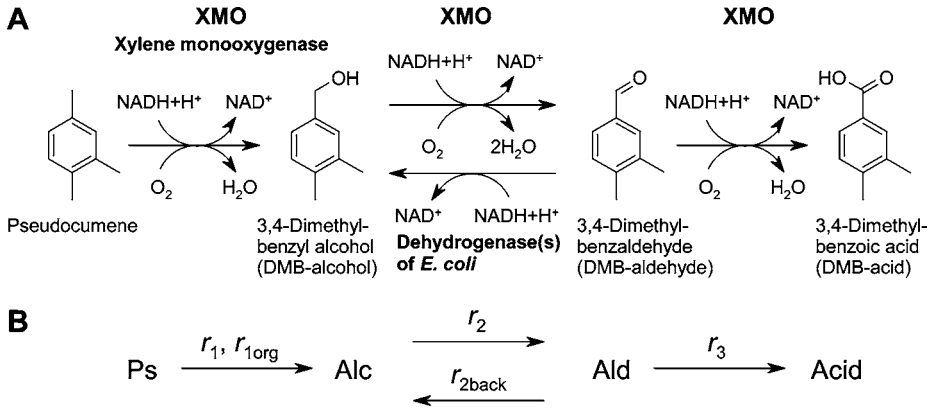

Figure 1. **Bioconversion reactions catalyzed by *E. coli* JM101 (pSPZ3). Panel A shows the consecutive oxygenation of pseudocumene to 3,4-dimethylbenzyl alcohol (DMB-alcohol), 3,4-dimethylbenzaldehyde (DMB-aldehyde), and 3,4-dimethylbenzoic acid (DMB-acid) catalyzed by xylene monooxygenase (XMO) and the back reaction from DMB-aldehyde to DMB-alcohol catalyzed by dehydrogenase(s) of the *E. coli* host. Panel B assigns the bioconversion rates r_1, r_{1org}, r_2, r_{2back}, and r_3 used in the modeling (see section 2) to the individual reaction steps. As in the subscripts of the modeling parameters, pseudocumene, DMB-alcohol, DMB-aldehyde, and DMB-acid are indicated as Ps, Alc, Ald, and Acid, respectively.**

The enzyme system, we use for this oxidation is the xylene monooxygenase (XMO) of *Pseudomonas putida* mt-2,[16,17] which consists of a NADH:acceptor reductase component (XylA)[18] and a membrane bound hydroxylase component (XylM).[19] This non-heme iron enzyme has a broad substrate range[20] and initiates xylene degradation by the specific hydroxylation of one methyl group.[21] We have demonstrated that recombinant *Escherichia coli* expressing the *xylMA* genes under control of the *alk* regulatory system[22] catalyze the monooxygenation not only of toluene and pseudocumene but also of the corresponding benzyl alcohols and benzaldehydes.[23] The kinetic analysis of this multistep reaction showed that the substrates toluene and pseudocumene as well as the corresponding alcohols inhibit aldehyde oxygenation and that elevated substrate concentrations also weakly inhibit alcohol oxygenation.[24] As an example for selective multistep biooxidation, we further investigated the bioconversion of pseudocumene to 3,4-dimethylbenzaldehyde (DMB-aldehyde) involving 3,4-dimethylbenzyl alcohol (DMB-alcohol) as intermediate and 3,4-dimethylbenzoic acid (DMB-acid) as potential byproduct (Figure 1 A). The development and optimization of a two-liquid-phase process with bis(2-ethylhexyl)phthalate (BEHP) as organic carrier solvent and recombinant *E. coli* as biocatalyst permitted directing this complex, kinetically controlled, multistep bioconversion to the exclusive production of the desired DMB-aldehyde.[25] Fed-batch growth guaranteed efficient NADH regeneration. Successful scale-up to technical scale and straightforward product purification resulted in the recovery of 469 g of DMB-aldehyde at a purity of 97% and an overall yield of 65%.[26]

Due to the lack of a comprehensive theory for such whole-cell biooxidations, process optimization has thus far been carried out by an empirical approach. The influence of important parameters has been investigated experimentally, and these parameters have been optimized one by one. This approach allowed obtaining suitable biotransformation conditions. A detailed process model based on knowledge gained by the empirical approach will facilitate process characterization and optimization especially when other substrates are used, leading to considerable savings in experimental effort and enabling a straightforward scale-up. Furthermore, such a mathematical model is a promising approach towards a comprehensive theory for whole-cell biooxidations in general.

The present article describes the development of a model for whole-cell biocatalysis in a two-liquid-phase system including cell growth and bioconversion kinetics. The primary goal is to use the model to further characterize and optimize the multistep biooxidation of pseudocumene to DMB-aldehyde in the BEHP-based two-liquid-phase system. The model allowed studying specific issues such as substrate transfer from the solvent to the cells, pH dependency, impact of the bioconversion on cell metabolism, the inhibitions of the different reaction steps by the reactants, and the impact of organic−aqueous mass transfer.

2. Modeling Aspects

The process model described in this work is designed for whole-cell biocatalysis in a stirred tank reactor containing a biphasic liquid consisting of aqueous minimal medium and an organic phase at a volume ratio of about 1:1.[24−26] Cells and the growth substrate, glucose, are considered to reside in the aqueous phase only. For the cells, no stable adsorption

(16) Worsey, M. J.; Williams, P. A. *J. Bacteriol.* **1975**, *124*, 7−13.
(17) Harayama, S.; Rekik, M.; Wubbolts, M.; Rose, K.; Leppik, R. A.; Timmis, K. N. *J. Bacteriol.* **1989**, *171*, 5048−5055.
(18) Shaw, J. P.; Harayama, S. *Eur. J. Biochem.* **1992**, *209*, 51−61.
(19) Shaw, J. P.; Harayama, S. *J. Ferm. Bioeng.* **1995**, *79*, 195−199.
(20) Wubbolts, M. G.; Reuvekamp, P.; Witholt, B. *Enzyme Microb. Technol.* **1994**, *16*, 608−615.
(21) Abril, M.-A.; Michan, C.; Timmis, K. N.; Ramos, J. L. *J. Bacteriol.* **1989**, *171*, 6782−6790.
(22) Panke, S.; Meyer, A.; Huber, C. M.; Witholt, B.; Wubbolts, M. G. *Appl. Environ. Microbiol.* **1999**, *65*, 2324−2332.
(23) Bühler, B.; Schmid, A.; Hauer, B.; Witholt, B. *J. Biol. Chem.* **2000**, *275*, 10085−10092.
(24) Bühler, B.; Witholt, B.; Hauer, B.; Schmid, A. *Appl. Environ. Microbiol.* **2002**, *68*, 560−568.
(25) Bühler, B.; Bollhalder, I.; Hauer, B.; Witholt, B.; Schmid, A. *Biotechnol. Bioeng.* **2003**, *81*, 683−694.
(26) Bühler, B.; Bollhalder, I.; Hauer, B.; Witholt, B.; Schmid, A. *Biotechnol. Bioeng.* **2003**, *82*, 833−842.

to and no partitioning into the organic phase were observed under the microscope. The biotransformation compounds are considered to partition between both phases.

2.1. Volume Calculation. Calculation of the concentration profiles during bioconversion requires knowledge of the phase volumes. The precise organic−aqueous volume ratio fluctuates during the experiments because the organic phase is added only after about 1 h, both phases are sampled, there is a feed of glucose during the experiment, pH control requires addition of acid or base, and some evaporation occurs. For calculation of the phase volumes, the two latter sources of volume change are neglected, since the volume changes caused thereby are minor. Furthermore, it is assumed that the reactions, phase mixing, mass transfer between the two phases, and temperature differences do not cause significant volume changes.

The volumes of the aqueous and organic phases are V^{aq} and V^{org}, respectively. The subscript 0 is used to indicate the initial volume, which for the aqueous phase is the volume at the beginning of fed-batch cultivation (t_0) and for the organic phase the volume at the time of its addition (t_{org}) to the fed-batch culture. The aqueous glucose feed flow F may be changing during the bioconversion and hence is a function of time. Both phases are sampled during the experiment at regular intervals. For simplicity, this is expressed as a continuous sample flow F_{sample}, the same for both phases. The volumes are calculated using the following equations:

$$V^{aq} = V_0^{aq} + (F - F_{sample})\cdot t \qquad [L_{aq}] \tag{1}$$

$$V^{org} = 0 \quad \text{for} \quad t < t_{org} \qquad [L_{org}] \tag{2.1}$$

$$V^{org} = V_0^{org} - F_{sample}\cdot t \quad \text{for} \quad t \geq t_{org} \qquad [L_{org}] \tag{2.2}$$

2.2. Biomass Growth. The bioconversion rates are proportional to the biomass concentration (C_X). Thus, a good prediction of C_X is needed, which is calculated using its macroscopic balance:

accumulation = production − flow out

$$\frac{d(V^{aq}\cdot C_X)}{dt} = V^{aq}\cdot r_X - F_{sample}\cdot C_X \qquad [g\ h^{-1}] \tag{3}$$

This equation can be integrated using the boundary condition $C_{X,0}$ at t_0. It is assumed that the rate of biomass accumulation (r_X) depends on the aqueous glucose concentration (C_{Glc}^{aq}) and the dissolved oxygen concentration ($C_{O_2}^{aq}$):

$$r_X = \frac{C_{Glc}^{aq}}{K_{s,Glc} + C_{Glc}^{aq}} \cdot \frac{C_{O_2}^{aq}}{K_{s,O_2} + C_{O_2}^{aq}} \cdot \mu_{max}\cdot C_X$$

$$[(g\ of\ CDW)\ L_{aq}^{-1}\ h^{-1}] \tag{4}$$

The Monod constants K_s are 0.0018 g L_{aq}^{-1} and 2×10^{-6} mmol L_{aq}^{-1} for glucose and oxygen, respectively.[27] Growth is also influenced by the biotransformation. The overproduction and presence of a heterologous monooxygenase as well as high bioconversion rates can have impeding or deleterious consequences for the host and its metabolism. This is due to additional protein synthesis, integration of enzyme components into the membrane, formation of reactive oxygen species, consumption of reducing equivalents (NADH), and the formation of toxic products, which need to be excreted.[28−32] Such effects lead to acetic acid formation and growth inhibition.[33] Due to yet insufficient knowledge in this context, bioconversion-related growth inhibition was only considered by varying the growth parameters μ_{max}, m_{Glc}, and $Y_{X/Glc}^{max}$ among and during the biotransformations depending on pH, time after induction, and scale. The growth parameters are summarized in Table 1 and discussed in section 3.2.

Table 1. **Growth parameters for the simulation of the reaction systems[a]**

		conditions	
parameter	unit	pH 7.1	pH 7.4
$K_{s,Glc}$	g L_{aq}^{-1}	0.0018	0.0018
K_{s,O_2}	mmol L_{aq}^{-1}	$2\cdot 10^{-6}$	$2\cdot 10^{-6}$
Initial μ_{max}	h^{-1}	0.38	0.34 (0.3)[b]
Initial m_{Glc}	g g^{-1} h^{-1}	0.01	0.04
$Y_{X/Glc}^{max}$ [c]	g g^{-1}	0.5	0.42 (0.33)[b]
$Y_{P/Glc}^{max}$	mmol $mCmol^{-1}$	1.67	1.67
Y_{P/O_2}^{max}	mmol $mmol^{-1}$	1	1
$(k_La)_{O_2}$ [d]	h^{-1}	1300 (1500)	1300 (1500)

[a] The growth parameters apply for the simulations using both models I and II for the rate equations of the biotransformation. [b] Values apply for the modeling of biotransformations on a 2-L scale. The numbers in parentheses apply to 30-L biotransformations. [c] Y_{X/O_2}^{max} is dependent on $Y_{X/Glc}^{max}$ as described in section 2 (eq 10). [d] $(k_La)_{O_2}$ values for cultivations on a 2-L scale at stirrer speeds of 2000 and 2500 rpm (brackets). $(k_La)_{O_2}$ values for cultivations on a 30-L scale are discussed in section 3.2.

2.3. Glucose Concentration. The glucose concentration is calculated using the following macroscopic balance:

accumulation = flow in − flow out − consumption

$$\frac{d(V^{aq}\cdot C_{Glc}^{aq})}{dt} = F\cdot C_{Glc}^{feed} - F_{sample}\cdot C_{Glc}^{aq} - V^{aq}\cdot r_{Glc} \qquad [g\ h^{-1}] \tag{5}$$

This equation can be integrated using the boundary condition $C_{Glc,0}^{aq} = 0$ at t_0. The feed flow contains the glucose concentration in the feeding solution C_{Glc}^{feed} (730 g L_{feed}^{-1}). The glucose consumption rate is described by:

$$r_{Glc} = \frac{r_X}{Y_{X/Glc}^{max}} + \frac{r_{P,NADH}}{Y_{P/Glc}^{max}} + m_{Glc}\cdot C_X \qquad [g\ L_{aq}^{-1}\ h^{-1}] \tag{6}$$

Thus, the glucose consumption depends on the maximum yields of biomass and biotransformation product on glucose $Y_{X/Glc}^{max}$ and $Y_{P/Glc}^{max}$, respectively, on the maintenance coefficient for glucose m_{Glc}, on the biomass formation rate r_X,

(27) Atkinson, B.; Mavituna, F. *Biochemical Engineering and Biotechnology Handbook*, 2nd ed.; Stockton Press: New York, 1991.

(28) Neubauer, P.; Lin, H. Y.; Mathiszik, B. *Biotechnol. Bioeng.* **2003**, *83*, 53−64.

(29) van Beilen, J. B.; Duetz, W. A.; Schmid, A.; Witholt, B. *Trends Biotechnol.* **2003**, *21*, 170−177.

(30) Nieboer, M.; Kingma, J.; Witholt, B. *Mol. Microbiol.* **1993**, *8*, 1039−1051.

(31) Chen, Q.; Janssen, D. B.; Witholt, B. *J. Bacteriol.* **1995**, *177*, 6894−6901.

(32) Chen, Q.; Janssen, D. B.; Witholt, B. *J. Bacteriol.* **1996**, *178*, 5508−5512.

(33) Park, J. B. *The Productivity of Biocatalytic Epoxidation of Styrene to (S)-Styrene Oxide*. Ph.D. Thesis, ETH Zurich, 2004.

and on the total NADH-coupled bioconversion rate $r_{P,NADH}$ which represents the sum of the rates of NADH consuming reaction steps including the oxygenation steps catalyzed by XMO and the back reaction from DMB-aldehyde to DMB-alcohol catalyzed by *E. coli* dehydrogenases ($r_{P,NADH} = r_1 + r_{1org} + r_2 + r_{2back} + r_3$, see Figure 1 and section 2.5).[23] An estimate for $Y^{max}_{P/Glc}$ is that per mole of glucose 10 moles of NADH can be produced by the microorganism; hence, $Y^{max}_{P/Glc}$ is 1.667 mol product per C-mol glucose. It must be considered that uncoupling of the bioconversion-related NADH oxidation from the biotransformation reactions may occur, thus leading to an underestimation of the bioconversion-related glucose consumption in the model. Furthermore, due to overflow metabolism and metabolic stress caused by the presence of the heterologous monooxygenase and high bioconversion rates (as mentioned above), glucose will be transformed into acetic acid or other metabolites instead of CO_2. Since the exact interrelationship of acetic acid formation is not known, this side reaction is not included in the model, leading to inaccuracies in the prediction of the glucose concentration.

2.4. Oxygen Concentration. Biomass growth also depends on the dissolved oxygen concentration. However, the dissolved oxygen tension (DOT) was generally maintained above 10% throughout the experimental biotransformations. Nevertheless, the oxygen concentration is considered in the model and is calculated using its macroscopic balance:

accumulation = oxygen transfer rate − consumption

$$\frac{d(V^{aq}\cdot C^{aq}_{O_2})}{dt} = V^{aq}\cdot\varphi_{O_2} - V^{aq}\cdot r_{O_2} \qquad [\text{mmol h}^{-1}] \qquad (7)$$

It is assumed that the influences of glucose feed and sampling are negligible. The oxygen concentration in equilibrium, $C^*_{O_2}$, is about 0.2−0.3 mmol L^{-1} in an aqueous fermentation medium aerated with air[34,35] and here was assumed to be 0.25 mmol L_{aq}^{-1}. Thus, eq 7 can be integrated using the boundary condition $C^{aq}_{O_2,0} = C^*_{O_2} = 0.25$ mmol L_{aq}^{-1} at t_0. The oxygen transfer rate from gas phase to aqueous phase is described by:

$$\varphi_{O_2} = (k_L a)_{O_2}\cdot(C^*_{O_2} - C^{aq}_{O_2}) \qquad [\text{mmol L}_{aq}^{-1}\,\text{h}^{-1}] \qquad (8)$$

In the presence of organic solvents, the volumetric mass transfer coefficient, $(k_L a)_{O_2}$, can be somewhat higher than usual. However, viscous organic solvents such as BEHP may impair mass transfer efficiency. For the lab-scale reactor used (2-L working volume) and aqueous medium, a maximal $(k_L a)_{O_2}$ of 1800 h^{-1} was estimated.[36] Here, based on the modeling of experimental biotransformations, we assumed a $(k_L a)_{O_2}$ of 1500 and 1300 h^{-1} at a stirrer speed of 2500 (maximum) and 2000 rpm, respectively. For simplicity, only maximal stirrer speeds were considered, and initial increases from lower stirrer speeds were neglected.

(34) Onken, U.; Liefke, E. *Adv. Biochem. Eng. Biotechnol.* **1989**, *40*, 137−166.
(35) Royce, P. C. N.; Thornhill, N. F. *AIChE J.* **1991**, *37*, 1680−1686.
(36) Schmid, A. *Two-Liquid-Phase Bioprocess Development; Interfacial Mass Transfer Rates and Explosion* Safety. Ph.D. Thesis, ETH Zurich, 1997.

The oxygen consumption rate (r_{O_2}) depends on the maximum yields of biomass and biotransformation product on oxygen Y^{max}_{X/O_2} and Y^{max}_{P/O_2}, respectively, biomass growth, maintenance, and the rates of all O_2-consuming oxidation steps catalyzed by XMO, r_1, r_{1org}, r_2, and r_3 (see section 2.5):

$$r_{O_2} = \frac{r_X}{Y^{max}_{X/O_2}} + \frac{r_1 + r_{1org} + r_2 + r_3}{Y^{max}_{P/O_2}} + m_{O_2}\cdot C_X \qquad [\text{mmol L}_{aq}^{-1}\,\text{h}^{-1}] \quad (9)$$

The maximum yield of biotransformation steps on oxygen $Y^{max}_{P/O_2} = 1$ mol mol^{-1} is derived from the stoichiometry of monooxygenases. The maximum yield of biomass on oxygen Y^{max}_{X/O_2} is derived from the stoichiometry of biomass formation assuming a biomass composition of $CH_{1.8}O_{0.5}N_{0.2}$:[27]

$$CH_2O + a\cdot O_2 + 0.2\cdot NH_3 \rightarrow Y^{max}_{X/Glc}\cdot CH_{1.8}O_{0.5}N_{0.2} + (1 - Y^{max}_{X/Glc})\cdot CO_2 + b\cdot H_2O$$

It can be derived that the coefficients for water and oxygen are $b = 1.3-0.9\cdot Y^{max}_{X/Glc}$ and $a = 1.15-1.2\cdot Y^{max}_{X/Glc}$. Then,

$$a = Y_{O_2/Glc} = \frac{Y^{max}_{X/Glc}}{Y^{max}_{X/O_2}}$$

so

$$Y^{max}_{X/O_2} = \frac{1}{\frac{1.15}{Y^{max}_{X/Glc}} - 1.2} \qquad [\text{mCmol mmol}^{-1}] \qquad (10)$$

The oxygen maintenance coefficient, m_{O_2}, can be derived from the stoichiometry of glucose respiration. This leads to:

$$m_{O_2}\,[\text{mmol mCmol}^{-1}\,\text{h}^{-1}] = m_{Glc}\,[\text{mCmol mCmol}^{-1}\,\text{h}^{-1}] \quad (11)$$

It must be considered that uncoupling of O_2 consumption from monooxygenation in XMO catalysis and acetic acid formation (see above) may result in an error in predictions of the oxygen concentration.

2.5. Biotransformation. The biotransformation compounds are pseudocumene, 3,4-dimethylbenzyl alcohol (DMB-alcohol), 3,4-dimethylbenzaldehyde (DMB-aldehyde), and 3,4-dimethylbenzoic acid (DMB-acid), indexed in the bioconversion parameters by the subscripts Ps, Alc, Ald, and Acid, respectively (Figure 1). The reaction rates between these compounds are sequentially r_1, r_2, and r_3. In contrast to glucose and the cells, the biotransformation compounds will be partly in the organic phase. For pseudocumene, we assume uptake also from the organic phase (see section 3.1.2) and release as DMB-alcohol into the aqueous phase. Thus, r_1 is split into an apparent rate for pseudocumene uptake from the organic phase r_{1org} and an apparent rate for pseudocumene uptake from the aqueous phase r_1 (Figure 1 B). Furthermore, a dehydrogenation-type back reaction from aldehyde to alcohol occurs in *E. coli*.[23] Thus, r_2 is split into

r_2 (forward reaction) and r_{2back} (reverse reaction) (Figure 1 B). The species balances for the aqueous phase are:

accumulation = transfer rate − flow out + production − consumption

$$\frac{d(V^{aq}\cdot C_{Ps}^{aq})}{dt} = V^{aq}\cdot\varphi_{Ps} - F_{sample}\cdot C_{Ps}^{aq} - V^{aq}\cdot r_1 \qquad [\text{mmol h}^{-1}] \quad (12.1)$$

$$\frac{d(V^{aq}\cdot C_{Alc}^{aq})}{dt} = V^{aq}\cdot\varphi_{Alc} - F_{sample}\cdot C_{Alc}^{aq} + V^{aq}\cdot(r_1 + r_{1org} - r_2 + r_{2back}) \qquad [\text{mmol h}^{-1}] \quad (12.2)$$

$$\frac{d(V^{aq}\cdot C_{Ald}^{aq})}{dt} = V^{aq}\cdot\varphi_{Ald} - F_{sample}\cdot C_{Ald}^{aq} + V^{aq}\cdot(r_2 - r_{2back} - r_3) \qquad [\text{mmol h}^{-1}] \quad (12.3)$$

$$\frac{d(V^{aq}\cdot C_{Acid}^{aq})}{dt} = V^{aq}\cdot\varphi_{Acid} - F_{sample}\cdot C_{Acid}^{aq} + V^{aq}\cdot r_3 \qquad [\text{mmol h}^{-1}] \quad (12.4)$$

These equations can be integrated using the boundary conditions $C_0^{aq} = 0$ at t_{org}.

Since pseudocumene is volatile, pseudocumene evaporation from the organic phase is considered. The pseudocumene evaporation rate is described by:

$$\varphi_{evap} = k_{evap}\cdot C_{Ps}^{org} \qquad [\text{mmol L}_{org}^{-1}\,\text{h}^{-1}] \quad (13)$$

The evaporation rate constant for pseudocumene (k_{evap}) calculated from the reactant balances in the biotransformation experiments amounts to 0.025 h^{-1}. Alternatively, assuming ideal conditions and that the air flow leaving the reactor is saturated with pseudocumene, the evaporation rate can be calculated on the basis of the aeration rate, the vapor pressure of pure pseudocumene, and the mole fraction at which pseudocumene is present in the organic phase. The vapor pressure of pure pseudocumene at 25 °C is 2.1 mmHg (http://esc.syrres.com/interkow/physdemo.htm) and was estimated to be 2.6 mmHg at 30 °C according to the equation of Clausius−Clapeyron. When a constant aeration rate of 1.5 L_{air} min^{-1} L_{org}^{-1} is assumed (the experimental aeration rate varied between 1 and 2 L_{air} min^{-1} L_{org}^{-1}), this gives an estimated evaporation rate constant of 0.0069 h^{-1}. This value is in the same order of magnitude but about 3 times lower than the experimental k_{evap}, which can be attributed to the nonideal conditions in the gaseous and liquid phases during the biotransformation.

The species balance for pseudocumene in the organic phase is:

accumulation = − transfer rate − flow out − consumption − evaporation

$$\frac{d(V^{org}\cdot C_{Ps}^{org})}{dt} = -V^{aq}\cdot\varphi_{Ps} - F_{sample}\cdot C_{Ps}^{org} - V^{aq}\cdot r_{1org} - V^{org}\cdot\varphi_{evap} \qquad [\text{mmol h}^{-1}] \quad (14.1)$$

This equation can be integrated using the boundary condition $C_{Ps,0}^{org}$ at t_{org}. Analogous equations apply to DMB-alcohol, DMB-aldehyde, and DMB-acid in the organic phase, but their initial concentrations will be zero and there will be no consumption and no evaporation (low volatilities).

The transfer rate of substrate and products from the organic to the aqueous phase is:

$$\varphi_a = (k_L a)_{org/aq}\cdot\left(\frac{C_a^{org}}{K_{p,a}} - C_a^{aq}\right) [\text{mmol L}_{aq}^{-1}\,\text{h}^{-1}] \quad (15)$$

The subscript a refers to the biotransformation compound considered. The mass transfer coefficient $(k_L a)_{org/aq}$ was assumed to be the same for all reactants and similar to the oxygen mass transfer coefficient (1300−1500 h^{-1}). On a technical scale, a significantly lower $(k_L a)_{org/aq}$ of 500 h^{-1} was assumed. Such values for $(k_L a)_{org/aq}$ are in the same range as reported for other two-liquid-phase processes performed in stirred-tank reactors with similar reactants, considering the varying power input in the different systems.[37−39] Furthermore, a sensitivity analysis will be presented for $(k_L a)_{org/aq}$. The molar partition coefficients of the substrate and products between the organic and aqueous phase, $K_{p,a}$, have been determined in an earlier study.[25]

For the rate equations of the biotransformation, two different models are used.

Model I. The first model involves Michaelis−Menten equations for r_1, r_{1org}, r_2, r_{2back}, and r_3, considering inhibition terms for the individual reactants. Evidence for such inhibitions was presented earlier.[23−25] Since these results indicated that the inhibitions are not purely competitive, rate equations including competitive (eq 16.1) and non competitive (eq 16.2) inhibitions were formulated and tested.

$$r_n = \frac{q_{max,n}\cdot\dfrac{C_a^{aq}}{K_{m,a}}\cdot C_X}{1 + \dfrac{C_a^{aq}}{K_{m,a}} + \dfrac{C_b^{aq}}{K_{i,b,n}}} \qquad [\text{mmol L}_{aq}^{-1}\,\text{h}^{-1}] \quad (16.1)$$

$$r_n = \frac{q_{max,n}\cdot\dfrac{C_a^{aq}}{K_{m,a}}\cdot C_X}{1 + \dfrac{C_a^{aq}}{K_{m,a}} + \dfrac{C_b^{aq}}{K_{i,b,n}} + \dfrac{C_a^{aq}\cdot C_b^{aq}}{K_{m,a}\cdot K_{i,b,n}}} [\text{mmol L}_{aq}^{-1}\,\text{h}^{-1}] \quad (16.2)$$

The subscripts a and b mark the parameters for the transformed and the inhibiting compound, respectively, and *n* the number of the reaction step considered. In the absence of inhibiting compounds, these equations become normal Michaelis−Menten equations. The Michaelis−Menten constants K_m and the maximal reaction velocities q_{max} for r_1, r_2, and r_3 are taken from an earlier study,[24] where q_{max} was termed V_{max}, assuming that the substrate uptake constants K_s given in that study are actually K_m values. For r_{1org}, a Michaelis−Menten equation including the same q_{max} as for r_1 and a constant specific for substrate uptake directly from the organic phase, $K_{m,Ps,org}$, is assumed. Whereas r_1, r_{1org}, and

(37) Cruickshank, S. M.; Daugulis, A. J.; McLellan, P. J. *Biotechnol. Bioeng.* **2000**, *67*, 224−233.
(38) Willeman, W. F.; Straathof, A. J. J.; Heijnen, J. J. *Enzyme Microb. Technol.* **2002**, *30*, 200−208.
(39) Willeman, W. F.; Gerrits, J. P.; Hanefeld, U.; Brussee, J.; Straathof, A. J. J.; van der Gen, A.; Heijnen, J. J. *Biotechnol. Bioeng.* **2002**, *77*, 239−247.

r_{2back} are supposed to be free of inhibitions by other reactants, r_2 is assumed to be noncompetitively inhibited by pseudocumene[24] and competitively or noncompetitively inhibited by the product DMB-aldehyde. The rate for the third reaction, r_3, is assumed to be noncompetitively inhibited by pseudocumene and DMB-alcohol.[24] The inhibition constants, $K_{i,b,n}$, as well as $K_{m,Ps,org}$ were obtained by model fitting. For r_{2back}, a normal Michaelis−Menten equation was used, neglecting the forward reaction DMB-alcohol → DMB-aldehyde in the dehydrogenation equilibrium. This is considered appropriate since an equilibrium constant of 0.01 was estimated for the dehydrogenase reaction catalyzed by *E. coli* (pSPZ3).[23] The parameters $q_{max,2back} = 13.9 \pm 2.1$ U (g of CDW)$^{-1}$ $= 0.83 \pm 0.13$ mmol (g of CDW)$^{-1}$ h^{-1} and $K_{m,Ald,back}$ ($=K_{s,Ald,back}$) $= 0.24 \pm 0.07$ mM were determined in this study as described in section 5.4.

Model II. The second model considers that biotransformation and oxidative phosphorylation, in which NADH is consumed for energy (ATP) generation, compete for NADH. The rates of both may be decreased by high overall biotransformation rates causing NADH shortage.[33] Since intracellular NADH concentrations are not known, NADH could not be introduced as a substrate into the rate equations of the biotransformation. As a modeling tool, we tentatively introduced a "feedback inhibition" of the individual oxygenation reactions and called it metabolic inhibition. This metabolic inhibition is assumed to be a noncompetitive type of inhibition of the XMO-catalyzed reactions by the total biotransformation-related NADH consumption rate $r_{P,NADH} = r_1 + r_{1org} + r_2 + r_{2back} + r_3$. Furthermore, a metabolic inhibition coefficient M_i (the same for all reaction steps) is introduced. Then, e.g., the equation for r_1 becomes:

$$r_1 = \frac{q_{max,1} \cdot \frac{C_{Ps}^{aq}}{K_{m,Ps}} \cdot C_X}{1 + \frac{C_{Ps}^{aq}}{K_{m,Ps}} + \frac{r_{P,NADH}}{M_i} + \frac{C_{Ps}^{aq} \cdot r_{P,NADH}}{K_{m,Ps} \cdot M_i}} \text{ [mmol } L_{aq}^{-1} \text{ h}^{-1}\text{]} \quad (17)$$

Analogous equations apply to r_{1org}, r_2, and r_3. A potential metabolic inhibition of r_{2back}, which is catalyzed by dehydrogenase(s) of *E. coli* and not by XMO, would necessitate a different specific metabolic inhibition constant. For simplicity and because of the low absolute rate of this reaction, such a potential metabolic inhibition was neglected.

The rates except for r_{2back} will depend on the dissolved oxygen concentration. Since oxygen was not limiting in experimental biotransformations, this dependence is neglected. Furthermore, it must be considered that, in the beginning of the experimental bioconversions, full induction of the XMO activity only was reached after 1−2 h. This induction phenomenon was not included in the model. However, due to the low initial cell (biocatalyst) concentrations, the induction kinetics had only a minor impact on the bioconversion pattern. The bioconversion parameters for the simulation of the reaction systems according to model II for the rate equations are summarized in Table 2 and discussed in section 3.2.

Table 2. **Bioconversion parameters for the simulation of the reaction systems according to model II for the rate equations[a]**

parameter	value	standard deviation[b]	unit
$q_{max,1}$	21.06	0.48	mmol (g of CDW)$^{-1}$ h^{-1}
$q_{max,2}$	5.58	0.18	mmol (g of CDW)$^{-1}$ h^{-1}
$q_{max,2back}$	0.83	0.13	mmol (g of CDW)$^{-1}$ h^{-1}
$q_{max,3}$	72		mmol (g of CDW)$^{-1}$ h^{-1}
$K_{m,Ps}$	0.202	0.008	mmol L_{aq}^{-1}
$K_{m,Alc}$	0.024	0.004	mmol L_{aq}^{-1}
$K_{m,Ald,back}$	0.24	0.07	mmol L_{aq}^{-1}
$K_{m,Ald}$	1		mmol L_{aq}^{-1}
$K_{m,Ps,org}$	850−1000		mmol L_{org}^{-1}
$K_{i,Ps,2}$	0.03		mmol L_{aq}^{-1}
$K_{i,Ald,2}$	0.004		mmol L_{aq}^{-1}
$K_{i,Ps,3}$	0.0002		mmol L_{aq}^{-1}
$K_{i,Alc,3}$	0.002		mmol L_{aq}^{-1}
k_{evap}	0.0069		h^{-1}
M_i			
pH 7.1	1.08		mmol (g of CDW)$^{-1}$ h^{-1}
pH 7.4	8.4		mmol (g of CDW)$^{-1}$ h^{-1}
$K_{p,Ps}$	24300	1500	L_{aq} L_{org}^{-1}
$K_{p,Alc}$	50	3	L_{aq} L_{org}^{-1}
$K_{p,Ald}$	906	20	L_{aq} L_{org}^{-1}
$K_{p,Acid}$	0.118	0.005	L_{aq} L_{org}^{-1}
$(k_La)_{org/aq}$			
2-L scale	1300 (1500)[c]		h^{-1}
30-L scale	500		h^{-1}

[a] All inhibition constants apply to noncompetitive inhibitions except for $K_{i,Ald,2}$, which applies to a competitive inhibition. The growth parameters used are listed in Table 1. CDW: cell dry weight. [b] As experimentally determined. [c] $(k_La)_{org/aq}$ values at a stirrer speed of 2000 and 2500 rpm (parentheses).

2.6. Simulation Procedure. The left-hand side of the aforementioned macroscopic balances was transformed into:

$$\frac{d(V \cdot C)}{dt} = V \cdot \frac{dC}{dt} + C \cdot \frac{dV}{dt} \quad (18)$$

Since the volume is known as a function of time according to eqs 1, 2.1, or 2.2, differential equations can be obtained, in which dC/dt is explicit. As a representative example for all balance equations, the equation for the aqueous glucose concentration becomes:

$$\frac{dC_{Glc}^{aq}}{dt} = \frac{F \cdot C_{Glc}^{feed} - F_{sample} \cdot C_{Glc}^{aq} - V^{aq} \cdot r_{Glc} - C_{Glc}^{aq} \cdot \frac{dV^{aq}}{dt}}{V^{aq}} = -r_{Glc} + \frac{F \cdot (C_{Glc}^{feed} - C_{Glc}^{aq})}{V^{aq}} \quad (19)$$

3. Results and Discussion

In prior studies, we reported that the two-liquid-phase concept allowed the exploitation of the complex kinetics of the multistep oxygenation of xylenes for the accumulation of one specific oxidation product, e.g., 3,4-dimethylbenzaldehyde from pseudocumene.[24,25] We now discuss general biotransformation aspects as a basis for our mathematical model, which describes biotransformation experiments performed at varying pH, scale, and substrate concentrations and builds on kinetic analyses. In part, the respective experimental results have been presented earlier.[24−26] Fol-

Table 3. **Process characteristics of representative biotransformations[a]**

parameter	unit	biotransformation I[b]	II[c]	III[c]	IV[c]
initial $[pseudocumene]_{org}$	mmol L_{org}^{-1}	315	500	400	355
working volume	L_{tot}	2	2	30	30
pH		7.1	7.4	7.4	7.1→7.4
growth rate[d]	h^{-1}	0.35	0.24	0.25	0.34
maximal CDW reached	(g of CDW) L_{aq}^{-1}	30	18	15.5	20
final $[DMB\text{-}aldehyde]_{org}$	mmol L_{org}^{-1}	220	330	254	274
product share in all reactants[e]	%	92	80	76	97
maximal specific pseudocumene oxidation rate	U (g of CDW)$^{-1}$	27	61	65	51
maximal specific DMB-aldehyde formation rate	U (g of CDW)$^{-1}$	16	43	36	30
maximal volumetric DMB-aldehyde formation rate	U L_{aq}^{-1}	390	710	440	500
average volumetric DMB-aldehyde formation rate	U L_{aq}^{-1}	244	416	293	325

[a] All experiments were carried out with BEHP as organic carrier solvent and at a phase ratio of 1:1. Initial pseudocumene concentration, scale, and pH varied.[25,26] CDW: cell dry weight. Subscripts: org: organic phase; aq: aqueous phase; tot: total volume. [b] Adapted from ref 25. [c] Adapted from ref 26. [d] Approximation for the exponential growth phase. [e] In the organic phase at the end of the biotransformation.

lowing that section, we present and discuss the modeling and simulation results for four representative biotransformations (referred to as biotransformations I, II, III, and IV throughout the paper) with characteristic process parameters summarized in Table 3.

3.1. Basic Considerations.

3.1.1. Solvent-Cell Mass Transfer. Volumetric productivities attained in two-liquid-phase systems can, in contrast to aqueous single-phase systems, be limited by the transport of substrates from an apolar phase to the cells residing in the aqueous phase. In our system, the maximal pseudocumene solvent−cell transfer rates amounted to 50 and 44 mmol L_{aq}^{-1} h^{-1} on a 2-L scale (at $C_X = 17.6$ (g of CDW) L^{-1} and $C_{Ps}^{org} = 244$ mM) and a 30-L scale (at $C_X = 14.3$ (g of CDW) L^{-1} and $C_{Ps}^{org} = 255$ mM), respectively. The independency on scale and the general dependency on cell and organic substrate concentrations as well as on pH[25,26] indicate that a potential absolute maximum of the volumetric solvent−cell transfer rate for pseudocumene was not reached. This is in agreement with results obtained by Schmid et al.,[40] who investigated a two-liquid-phase system with hexadecene as organic carrier solvent and, e.g., octane as growth substrate for *P. putida* GPo1. Despite the very high partition coefficient of 6.7×10^5 for octane and its very low water solubility of 5 μM, they found octane solvent−cell transfer rates of up to 30 mmol L_{aq}^{-1} h^{-1} at growth-limiting organic octane concentrations below 3% (vol/vol). Furthermore, their results suggested that growth was kinetically limited by a reduced octane-uptake capacity of the cells at low octane concentrations in the apolar phase[41,42] and not by an absolute maximum of the volumetric substrate mass transfer from the organic phase to the cells. Our results indicate that the same is true for pseudocumene bioconversion by *E. coli* JM101 (pSPZ3).

3.1.2. Substrate Uptake Mechanism. For a reasonable modeling of whole-cell-based bioconversions of apolar substrates such as pseudocumene, the type of substrate uptake mechanism is important. Three different bacterial uptake mechanisms for apolar hydrocarbons have been described, including uptake from the aqueous phase, uptake of solubilized substrates, and uptake via direct cellular contact with organic phase droplets.[36]

Uptake of substrates dissolved in the aqueous phase was reported for *n*-alkanes with chain lengths shorter than those of nonane,[40,43] cyclic hydrocarbons,[44,45] and toluene,[46] which is similar to pseudocumene but less hydrophobic. Different observations indicate that pseudocumene may not exclusively be taken up from the aqueous phase: The aqueous phase toxicity limit for pseudocumene in a two-liquid phase system is significantly lower than in an aqueous one-phase system and the product formation pattern does not only depend on the aqueous substrate concentration.[25] Furthermore, experimental pseudocumene oxidation rates at pH 7.1 tended to exceed maximal theoretical reaction rates calculated using the Lineweaver−Burk equation and aqueous pseudocumene concentrations derived from the partition coefficient and organic pseudocumene concentrations.[25] Note that the kinetic parameters used in the Lineweaver−Burk equation have been determined in an aqueous single-phase system. In biotransformations performed at pH 7.4 instead of 7.1, significantly higher bioconversion rates were achieved.[26] As shown in Figure 2, pseudocumene oxidation rates measured in laboratory- (Figure 2 A) as well as technical-scale (Figure 2 B) biotransformations performed at pH 7.4 clearly exceed the theoretical maxima. Thus, we conclude that uptake of pseudocumene dissolved in the aqueous phase cannot account for the total pseudocumene uptake by the cells in the BEHP-based two-liquid-phase system.

Hydrocarbon-assimilating bacteria are known to excrete surface-active compounds when grown in two-liquid-phase cultures.[47−49] Specific surfactants were reported to be neces-

(40) Schmid, A.; Sonnleitner, B.; Witholt, B. *Biotechnol. Bioeng.* **1998**, *60*, 10−23.
(41) Atherton, J. H. In *Research in Chemical Kinetics*, 2nd ed.; Compton, T. G., Hancock, G., Eds.; Elsevier: Amsterdam, 1994; pp 193−259.
(42) Moser, A. *Bioprocess Technology*; Springer-Verlag: Wien, 1981.
(43) Cameotra, S. S.; Singh, H. D. *J. Microb. Biotechnol.* **1990**, *5*, 47−57.
(44) Köhler, A.; Schüttoff, M.; Bryniok, D.; Knackmuss, H.-J. *Biodegradation* **1994**, *5*, 93−103.
(45) Sikkema, J.; de Bont, J. A. M.; Poolman, B. *Microbiol. Rev.* **1995**, *59*, 201−222.
(46) Woodley, J. M.; Brazier, A. J.; Lilly, M. D. *Biotechnol. Bioeng.* **1991**, *37*, 133−140.
(47) de Smet, M.-J.; Kingma, J.; Wynberg, H.; Witholt, B. *Enzyme Microb. Technol.* **1983**, *5*, 352−360.
(48) Desai, J. D.; Banat, I. M. *Microbiol. Mol. Biol. Rev.* **1997**, *61*, 47−64.

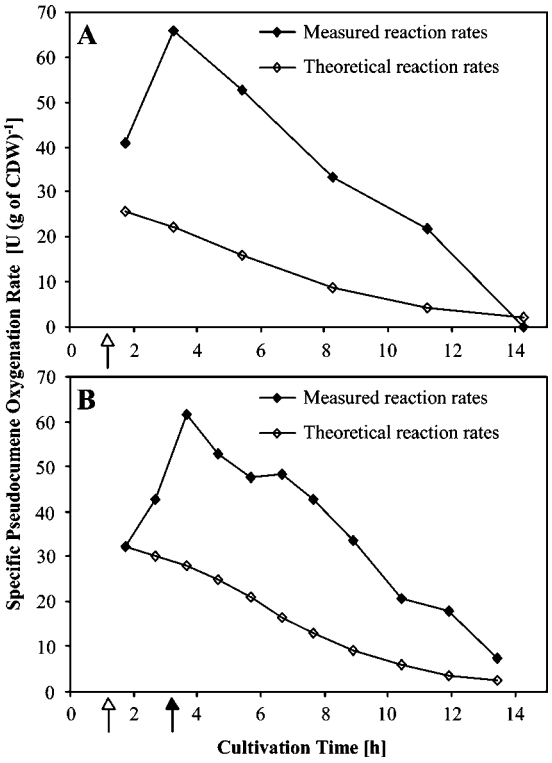

Figure 2. **Comparison of measured reaction rates of pseudocumene oxidation and theoretical values corresponding to maximally possible reaction rates calculated via Lineweaver−Burk equation and aqueous pseudocumene concentrations derived from the partition coefficient. Panels A and B show the results for biotransformations II performed on a 2-L scale at pH 7.4 and biotransformation IV performed on a 30-L scale and including pH shifts from 7.1 to 7.4, respectively (Table 3). The experimental two-liquid-phase biotransformations are based on *E. coli* JM101 (pSPZ3) growing in fed-batch mode as biocatalyst and BEHP as organic carrier solvent present at a phase ratio of 1:1 and containing, beside the substrate pseudocumene, 1% (vol/vol) *n*-octane for induction. Addition of the organic phase occurred after 1−1.33 h of fed-batch cultivation (open arrow). The closed arrow indicates the time point of the pH shift to pH 7.4 in biotransformation IV. Experimental details have been described.[26]**

sary for the efficient uptake of long-chain alkanes by various *Pseudomonas* and *Candida* species.[50−53] To our knowledge, such a specific excretion of biosurfactants is not known for *E. coli*. Furthermore, aqueous pseudocumene concentrations significantly higher than the theoretical values, which could be caused by solubilizing effects of cell lysis products and/or surface-active outer membrane compounds (polysaccharides, phospholipids, proteins),[54,55] were not measured.[25] Thus, substrate solubilization can be ruled out as a major mechanism for pseudocumene uptake.

Substrate uptake directly from the organic phase via cell−droplet interaction was assumed for substrates with low water solubilities, e.g., for long-chain alkanes,[40,56−58] menthyl acetate,[59] and trichlorophenol.[60] In our experiments, uptake via cell−droplet interactions would explain the observations that, in the two-liquid phase system, the aqueous toxicity limit seems to be much lower than in the aqueous single-phase system and that the product formation pattern does not directly depend on aqueous substrate concentrations. Such an uptake mechanism does not depend on mass transfer from the organic to the aqueous phase and would explain the relatively high pseudocumene oxidation rates in our experiments.

Thus, we conclude that the product formation rate is dependent on the amount of pseudocumene present in the organic phase and suggest that pseudocumene uptake occurs at least in part directly from the organic phase. This was included in the model by introducing two rates for the first reaction step, one for the reaction in the aqueous phase and one for pseudocumene uptake from the organic phase and DMB-alcohol release into the aqueous phase (see section 2.5).

3.1.3. pH Dependency and Metabolic Inhibition. The pH significantly influenced the reaction and growth rates as can be seen by considering the process parameters shown in Table 3. When the modeling is performed according to model I for the rate equations of the biotransformation (eqs 16.1 and 16.2), appropriate modeling results for all the different biotransformations considered can only be obtained by changing the kinetic parameters, thus accelerating the individual reaction steps at higher pH. Introduction of an influence of the pH on pseudocumene uptake from the organic phase and on the noncompetitive inhibitions of DMB-alcohol oxidation by pseudocumene and DMB-aldehyde delivered acceptable modeling results. Here, noncompetitive inhibition by DMB-aldehyde allowed better simulation results than competitive inhibition. At pH 7.4, the correct prediction of the biotransformation dynamics at different volumetric scales necessitated further adaptations of these kinetic parameters. The modeling parameters at varying pH and scale are summarized in Table 4. As an example, the simulation results for the 30-L scale biotransformation IV, including two pH shifts, are shown in Figure 3. At the time point of the second pH shift at 3.22 h of fed-batch cultivation, the parameters indicated in Table 4 were changed in one step, although the response to such pH shifts is expected to be rather continuous than immediate. Similarly to the nonimmediate induction, this inaccuracy was accepted for the modeling and resulted in a slight overestimation of the reaction rates in the beginning of the biotransformation. Good agreements of simulations with experimental results, as exemplified for biotransformation IV (Figure 3), were

(49) Schmid, A.; Kollmer, A.; Witholt, B. *Enzyme Microb. Technol.* **1998**, *22*, 487−493.
(50) Reddy, P. G.; Singh, H. D.; Roy, P. K.; Baruah, J. N. *Biotechnol. Bioeng.* **1982**, *24*, 1241−1269.
(51) Hardegger, M.; Koch, A. K.; Ochsner, U. A.; Fiechter, A.; Reiser, J. *Appl. Environ. Microbiol.* **1994**, *60*, 3679−3687.
(52) Sekelsky, A. M.; Shreve, G. S. *Biotechnol. Bioeng.* **1999**, *63*, 401−409.
(53) Noordman, W. H.; Wachter, J. H. J.; de Boer, G. J.; Janssen, D. B. *J. Biotechnol.* **2002**, *94*, 195−212.
(54) Hoekstra, D.; van der Laan, J. W.; de Leij, L.; Witholt, B. *Biochim. Biophys. Acta* **1976**, *455*, 889−899.
(55) Gankema, H.; Wensink, J.; Guinee, P. A. M.; Jansen, W. H.; Witholt, B. *Infect. Immun.* **1980**, *29*, 704−713.
(56) Neufeld, R. J.; Zajic, J. E.; Gerson, D. F. *J. Ferment. Technol.* **1983**, *61*, 315−321.
(57) Rosenberg, M.; Rosenberg, E. *J. Bacteriol.* **1981**, *148*, 51−57.
(58) Goswami, P. C.; Singh, H. D. *Biotechnol. Bioeng.* **1991**, *37*, 1−11.
(59) Westgate, S.; Bell, G.; Halling, P. J. *Biotechnol. Lett.* **1995**, *17*, 1013−1018.
(60) Ascón-Cabrera, M. A.; Lebeault, J.-M. *J. Ferment. Bioeng.* **1995**, *80*, 270−275.

Table 4. **Kinetic modeling parameters varied with pH and scale using model I for the rate equations of the bioconversion[a]**

		conditions		
parameter	unit	pH 7.1, both scales	pH 7.4, 2-L scale	pH 7.4, 30-L scale
$K_{m,Ps,org}$	mmol L_{org}^{-1}	4500	2400	1750
$K_{i,Ps,2}$	mmol L_{aq}^{-1}	0.0016	0.012	0.008
$K_{i,Ald,2}$	mmol L_{aq}^{-1}	0.045	0.19	0.09

[a] Both inhibition constants, for pseudocumene and DMB-aldehyde as inhibitors, apply to noncompetitive inhibitions of the second reaction step. For the rest of the bioconversion-related modeling parameters except for M_i, which is not considered in model I, the parameters given in Table 2 were applied. The growth parameters used are listed in Table 1.

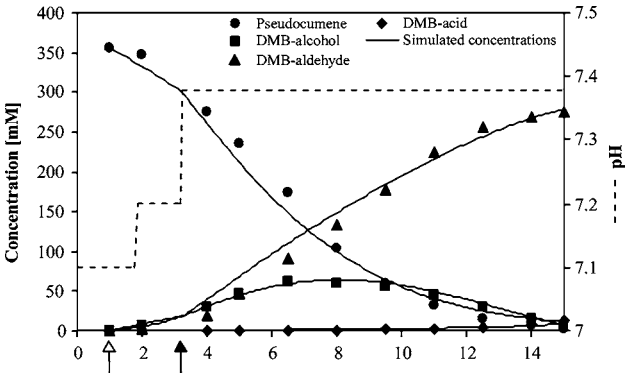

Figure 3. **Modeling results concerning the bioconversion in biotransformation IV using model I for the rate equations. Symbols and solid lines indicate experimental and simulated concentrations, respectively. Additionally, the course of the experimental pH is shown. The experimental two-liquid-phase biotransformation on a technical scale (30-L working volume) was performed as described for Figure 2 and earlier.[26] The open arrow indicates organic phase addition. The closed arrow shows the time point of the change of the modeling parameters as a consequence of the pH shift and according to Table 4. The values for all other modeling parameters concerning bioconversion (except for M_i, which is not included in model I for the rate equations) and growth are listed in Tables 2 and 1, respectively.**

obtained for all biotransformations presented earlier.[24−26] This supports the validity of the basic concept of the model formulation. However, it is improbable that pH and scale simultaneously influence substrate uptake and two inhibitions as assumed for the modeling based on model I for the rate equations.

To investigate the pH-dependent variance in specific biocatalyst activity, we performed short-term resting cell experiments (5 min of reaction) at varying pH: Exponentially growing cells were harvested, resuspended, and equilibrated in glucose-containing potassium phosphate buffer (see section 5.4). Except for pH values below 7, these experiments revealed only a small dependence of the specific rates of the three monooxygenation steps on pH, whereas a significant difference between pH 7.1 and 7.4 was observed in long-term biotransformation experiments with cells growing in fed-batch mode. Figure 4 shows this phenomenon for DMB-alcohol oxidation, which is not substrate limited in two-liquid-phase biotransformations. Long-term stability of specific activities necessitated the use of metabolically active,

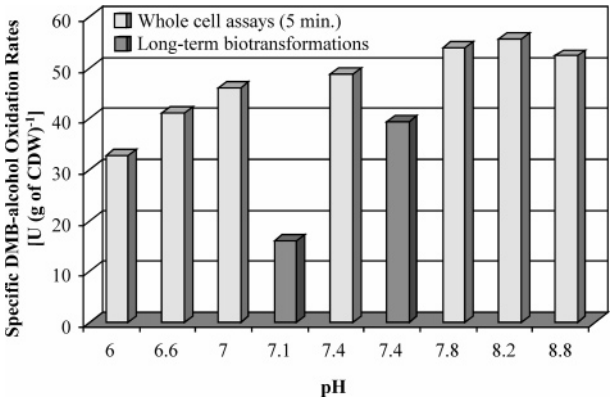

Figure 4. **Comparison of specific DMB-alcohol oxidation rates at varying pH achieved in short-termed (5 min) whole-cell activity assays with resting cells and in long-term two-liquid-phase biotransformations with growing cells. Experimental details are described in section 5.4.**

growing cells, allowing efficient NADH regeneration and was achieved by fed-batch cultivation.[25] Still, the higher specific activities in short-term resting cell biotransformations as compared to long-term biotransformations (Figure 4) may be explained by a better availability of the cofactor during short reaction times (5 min) and the lack of other NADH consuming oxidation steps such as pseudocumene oxygenation. Thus, the clear effect of the pH in long-term biotransformations and the lack of such an effect in short-term bioconversions points to an influence of the pH on NADH availability in growing cells. Biotransformation and oxidative phosphorylation, in which NADH is consumed for energy (ATP) generation, compete for NADH in growing cells. Both may be affected by high biotransformation rates causing metabolic stress and NADH shortage, especially at high overall reaction rates.[33] The prominent effect of the pH in such biotransformations (Figure 4) may be explained by an influence of the pH on the competition of XMO and oxidative phosphorylation for NADH. Increasing the pH might promote the flow of reduction equivalents (NADH) to XMO at the expense of the flow to the electron transport chain and thus cause additional stress for the cells and interfere with cell growth. This is reasonable since the pH influences the proton gradient and thus the proton motive force over the cytoplasmic membrane,[61,62] where the enzyme systems competing for NADH, namely XMO and the enzymes involved in oxidative phosphorylation, are located. In fact, growth is influenced by the higher biotransformation rate. Biomass yield and growth rate are lower at higher biotransformation rates.[26] To evaluate such an influence of the pH on the competition for NADH and since intracellular concentrations of this potentially limiting substrate were not known, we introduced an inhibition of the biooxidation rates by the total NADH-consuming biotransformation activity in model II for the rate equations of the biotransformation (eq 17). The extent of this so-called metabolic inhibition was assumed to vary with pH. The introduction of such a

(61) Slonczewski, J. L.; Rosen, B. P.; Alger, J. R.; Macnab, R. M. *Proc. Natl. Acad. Sci. U.S.A.* **1981**, *78*, 6271−6275.
(62) Zilberstein, D.; Agmon, V.; Schuldiner, S.; Padan, E. *J. Bacteriol.* **1984**, *158*, 246−252.

"feedback-inhibition" of the biotransformation rates as a modeling tool opened the possibility to simulate different degrees of NADH limitation at varying pH and, most importantly, allowed consistent process simulation with constant $K_{m,Ps,org}$, $K_{i,Ps,2}$, and $K_{i,Ald,2}$ at different conditions.

3.2. Modeling and Simulation Results. Growth parameters and the biotransformation parameters $K_{i,b,n}$, $K_{m,Ps,org}$, and M_i were fitted to be as consistent as possible for the different biotransformations including experiments performed with varying initial pseudocumene concentrations, at pH 7.1 and 7.4, and on a 2- and a 30-L scale.[25,26] The simulation results for four representative biotransformations (Table 3) are shown in Figures 5 and 6 and are discussed in more detail regarding cell growth, biotransformation pattern, the inhibition of the second oxidation step by DMB-aldehyde, and organic−aqueous mass transfer.

3.2.1. Cell Growth. The main goal of the modeling was to investigate the bioconversion characteristics of a whole-cell multistep biooxidation in a two-liquid-phase system on a theoretical level. The direct dependence of the volumetric bioconversion rates on biomass (biocatalyst) concentrations[25] necessitates the correct prediction of cell concentrations. Table 1 shows a summary of the parameters used to simulate cell growth during the biotransformations. Figure 5 shows the simulations of growth and glucose concentrations in four representative biotransformations. The pH influenced the growth behavior. At pH 7.4 as compared to pH 7.1, $Y^{max}_{X/Glc}$ and μ_{max} changed to lower and m_{Glc} to higher values (Table 1). At higher pH, apparently, more glucose was needed for growth and maintenance. These results are in accordance with an influence of the pH on the competition for NADH between XMO and oxidative phosphorylation, favoring NADH flux to XMO at higher pH and causing additional metabolic burden for the cells (such as extrusion of products, handling of reactive oxygen species) as assumed in model II for the rate equations of the bioconversion.

For the 2-L scale biotransformations at pH 7.1 and 7.4 (Figure 5 A and B, respectively), exponential as well as glucose-limited growth were well predicted by the model. However, after about 7 h of fed-batch cultivation and 6 h of biotransformation, cell growth slowed and stopped, which was not predicted by the model. Such transitions to the stationary phase may be caused, in addition to various effects observed in high cell density fed-batch cultures such as the occurrence of a nondividing cell population and cell lysis,[63] by metabolic stress due to *xylMA* expression, integration of XylM into the membrane, formation of reactive oxygen species, consumption of reducing equivalents (NADH) by XMO, and/or substrate and product toxicity.[28−32] These yet poorly defined influences on cell metabolism necessitated changes of μ_{max} (decrease to 0.01−0.03 h^{-1}) and m_{Glc} (increase to 0.2−0.3 g g^{-1} h^{-1}).

On a technical scale of 30-L working volume, glucose was present throughout the biotransformations (Figure 5 C and D). There, apart from changes of $Y^{max}_{X/Glc}$, m_{Glc}, and μ_{max} due to pH shifts and transition to the stationary phase, further parameter changes were necessary to predict correct cell and glucose concentrations. This points to a continuously changing growth behavior. To simulate cell growth in biotransformation III (Figure 5 C), two changes of μ_{max} and m_{Glc} were introduced. After 4 h of cultivation, m_{Glc} was increased to 0.12 g g^{-1} h^{-1}, and μ_{max} was lowered to 0.1 h^{-1}. The

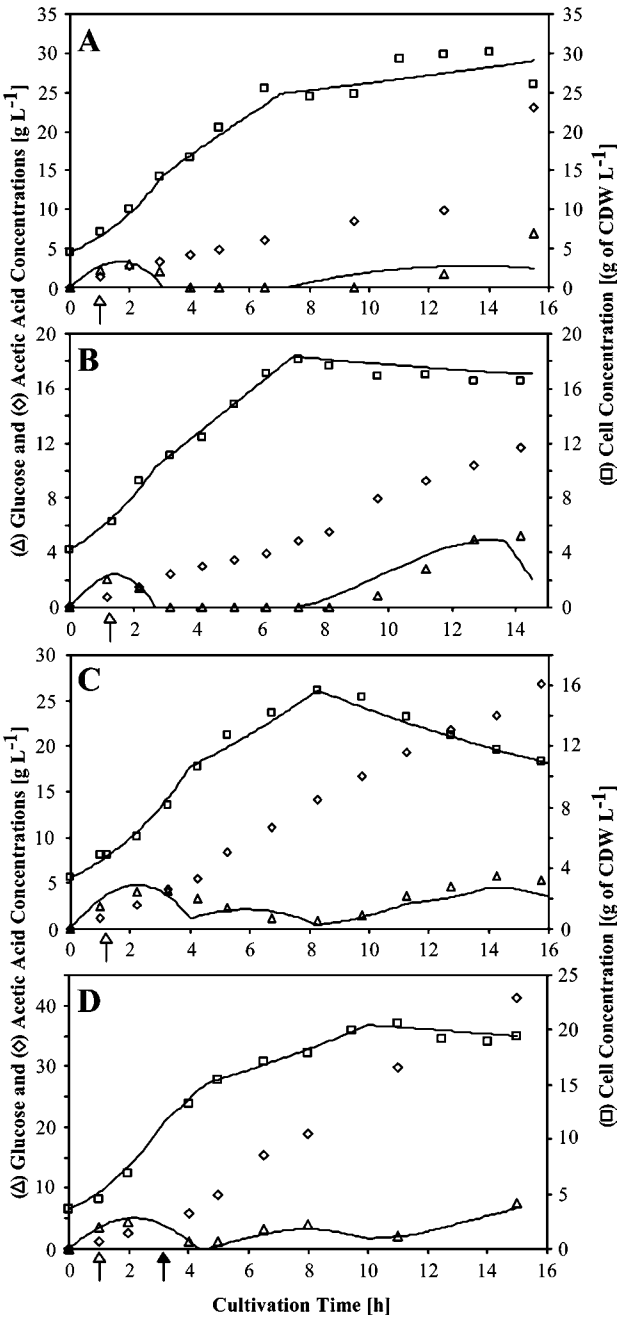

Figure 5. **Simulation of growth and glucose concentrations during biotransformations I (A), II (B), III (C), and IV (D). Simulated cell and glucose concentrations did not substantially differ for model I or II for the rate equations of the bioconversion. Symbols show experimentally measured and solid lines simulated values. The experimental two-liquid-phase biotransformations were performed as described for Figure 2 and earlier.[25,26] Open arrows indicate organic phase addition. The closed arrow in panel D shows the time point of the change of the modeling parameters as a consequence of the pH shifts in biotransformation IV. Growth and bioconversion parameters used for the simulations are shown in Tables 1 and 2, respectively.**

(63) Andersson, L.; Strandberg, L.; Enfors, S.-O. *Biotechnol. Prog.* **1996**, *12*, 190−195.

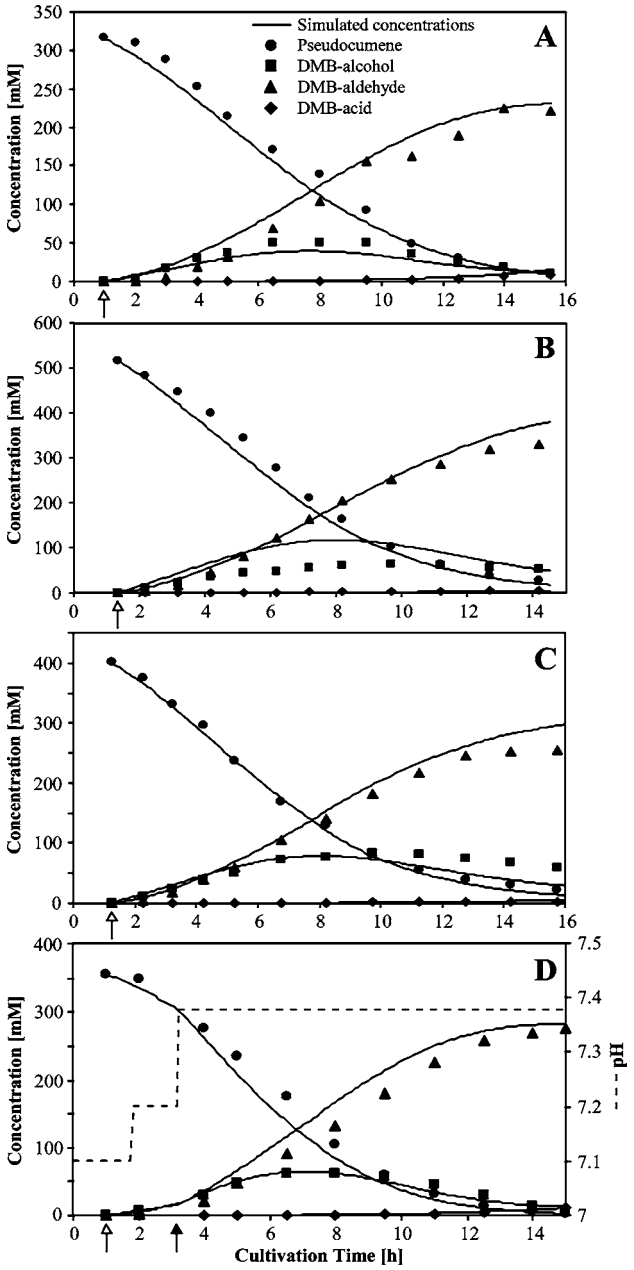

Figure 6. **Simulation results concerning the bioconversion in biotransformations I (A), II (B), III (C), and IV (D). Symbols and solid lines indicate experimental and simulated concentrations, respectively. Panel D additionally shows the course of the experimental pH in biotransformation IV. The experimental two-liquid-phase biotransformations were performed as described for Figure 2 and earlier.[25,26] Open arrows indicate organic phase addition. Closed arrows indicate the change of the modeling parameters as a consequence of the pH shifts. Growth and bioconversion parameters used for the simulations are shown in Tables 1 and 2, respectively.**

transition to the stationary phase, in which a significant reduction of the cell concentration occurred, was considered by decreasing μ_{max} to a negative value (-0.04 h^{-1}) and increasing m_{Glc} to 0.31 g g^{-1} h^{-1}. For biotransformation IV (Figure 5 D), after 3.22 h of fed-batch cultivation (shift to pH 7.4), $Y^{max}_{X/Glc}$, m_{Glc}, and μ_{max} were changed to 0.33 g g^{-1}, 0.04 g g^{-1} h^{-1}, and 0.2 h^{-1}, respectively. After 4.7 h of cultivation, m_{Glc} was increased to 0.15 g g^{-1} h^{-1}, and μ_{max} was lowered to 0.067 h^{-1}. Finally, the transition to the stationary phase was considered by decreasing μ_{max} to 0 h^{-1} and increasing m_{Glc} to 0.28 g g^{-1} h^{-1}. The generally lower μ_{max} and $Y^{max}_{X/Glc}$ at pH 7.4 on technical scale as compared to pH 7.4 on laboratory scale may be explained by the higher acetic acid formation rate, which may be due to the presence of glucose throughout the biotransformations, resulting in growth inhibition and less efficient glucose utilization.[64] Furthermore, also initial μ_{max} and $Y^{max}_{X/Glc}$ were slightly lower at technical scale as compared to laboratory scale (Table 1), which can be explained by a glucose gradient formation lowering cell yield and increasing acetic acid formation.[65,66]

As mentioned in section 2, only vague predictions of the oxygen concentration were possible due to the unknown interrelationship between recombinant oxygenase production, bioconversion, and metabolic stress. However, qualitatively, the predicted dissolved oxygen concentration kinetics correlated with the measured dissolved oxygen tension kinetics, when we consider that the discontinuous changes of the growth parameters in the model actually are continuous dynamic changes (results not shown). Quantitatively, the predicted oxygen concentrations at pH 7.4 and 7.1 tended to be too low and slightly too high, respectively, when compared with the measured oxygen tensions. These results again point to a significant influence of the pH on cell metabolism during biotransformation.

The modeling of cell growth necessitates yet undefined adaptations of growth parameters, is thus still suboptimal, and needs improvement in order to be applied for optimizing the growth conditions. Nevertheless, it meets the preliminary goal, the adequate simulation of biocatalyst concentrations, and allows the conclusion that biotransformation and pH have an impact on cell metabolism and thus growth.

3.2.2. Product Formation Pattern and Biotransformation Rates. Figure 6 shows the simulations of pseudocumene bioconversion in biotransformations I−IV according to model II for the rate equations. The bioconversion parameters used for the simulations are given in Table 2 and allowed appropriate predictions of the biotransformation rates at pH 7.1 and 7.4 using a single set of kinetic parameters. The only parameter, which was changed with pH, was the metabolic inhibition coefficient M_i introduced in eq 17. With an M_i of 18 U (g of CDW)$^{-1}$ = 1.08 mmol (g of CDW)$^{-1}$ h^{-1} for biotransformation I at pH 7.1, substrate and product concentrations were simulated well with a minor deviation at the beginning due to the neglect of induction kinetics (Figure 6 A). At pH 7.4, a significantly higher M_i of 140 U (g of CDW)$^{-1}$ = 8.4 mmol (g of CDW)$^{-1}$ h^{-1} resulted in good simulation results. For biotransformation II (Figure 6 B), the transient DMB-alcohol accumulation was somewhat overestimated, which involved an underestimation of the specific DMB-alcohol oxidation rate. Towards the end of this biotransformation and of biotransformation III (Figure 6 C), in which the transient DMB-alcohol accumulation was well

(64) Aristidou, A. A.; San, K.-Y.; Bennet, G. N. *Biotechnol. Bioeng.* **1999**, *63*, 737−749.
(65) Bylund, F.; Collet, E.; Enfors, S.-O.; Larsson, G. *Bioprocess Eng.* **1998**, *18*, 171−180.
(66) Neubauer, P.; Häggström, L.; Enfors, S.-O. *Biotechnol. Bioeng.* **1995**, *47*, 139−146.

predicted, the experimental reaction rates fell below the simulated rates, which may be due to the low metabolic activity of stationary-phase cells and thus to an impaired NADH regeneration. Such an increased loss of viability at pH 7.4 is in accordance with the higher impact of bioconversion on growth as discussed above and the decreasing cell concentrations at the end of, e.g., biotransformation III (Figure 5 C). Thus, the reduced NADH regeneration capacity in the stationary phase, as discussed for the transition to the stationary phase (see above), might be a consequence of the stress associated with the production and presence of heterologous proteins, especially of active membrane associated monooxygenases,[28−32] and with the high biotransformation rates causing significant production of toxic compounds and NADH shortage. As a consequence, a high pH as compared to a low pH results in a beneficial as well as an unfavorable effect on biotransformation efficiency. The beneficial effect is that higher specific activities of the biocatalyst can be reached during fed-batch growth. The adverse effect is the more pronounced stress for the host cells and the concomitant reduction of viability, which leads to lower biocatalyst concentrations and an earlier loss of biocatalyst activity.

However, as indicated by biotransformation IV, the regulation of the pH during the process may allow profiting from beneficial effects while minimizing unfavorable effects. A single change of M_i after 3.22 h resulted in appropriate simulation of substrate and product concentrations (Figure 6 D), although the response to the pH shifts is expected to be rather continuous than immediate. As compared to the simulation using model I for the rate equations (Figure 3), the predicted course of the specific reaction rates was more accurate (results not shown). Combined with the use of a single set of bioconversion parameters except for M_i, this demonstrates the superiority of model II over model I for the rate equations and supports a potential influence of the pH on the competition for NADH between XMO and the respiratory chain. This competition may be influenced by a pH-dependent variation of expression level, stability, or activity of XMO or of the enzymes involved in oxidative phosphorylation. A pH dependency of XMO activity can be ruled out since the pH did not significantly influence the specific rate of DMB-alcohol oxidation in activity assays (Figure 4) and since a pH optimum of 7 has been reported for partly purified XMO.[19] A pH dependence of the expression level of NADH-dependent metabolic enzymes has been reported.[67] However, the exact nature of the effect of the pH on biotransformation and cell growth remains to be investigated. This might lead to an improved model especially concerning cell growth. The high accuracy of the simulation results presented here illustrates the potential of the model for future process optimization.

3.2.3. Inhibition of DMB-Alcohol Oxidation by DMB-Aldehyde. All inhibitions exerted by pseudocumene and DMB-alcohol have been described in earlier studies.[23−25] Here, reasonable simulation of DMB-alcohol oxidation necessitated the introduction of an additional inhibition by DMB-aldehyde into the model. When model I for the rate equations was used for simulation, the best results were obtained by assuming a noncompetitive inhibition of the second reaction step by its product. In contrast, model II for the rate equations indicated a competitive type of inhibition. To prove the existence of such an inhibition and to gain insight into its characteristics, we experimentally analyzed the kinetics of the second oxygenation step in detail. We determined apparent maximal reaction velocities ($q_{max,2}$) and substrate uptake constants ($K_{s,Alc}$) for *E. coli* JM101 (pSPZ3) at various initial DMB-aldehyde concentrations (Table 5). At all inhibitor concentrations, the cells showed Michaelis−Menten-like kinetics for DMB-aldehyde formation from DMB-alcohol. The corresponding Lineweaver−Burk plots are shown in Figure 7. The curves fitted according to the weighted parameters $q_{max,2}$ and $K_{s,Alc}$ tend to intersect next to the *y* axis as expected from the low variance of the apparent $q_{max,2}$ and the high variance of the apparent $K_{s,Alc}$ with inhibitor concentration (Table 5). This points to a competitive inhibition of the second step by its product as suggested by model II for the rate equations. However, mixed-type inhibition with a strong contribution of competitive inhibition cannot completely be ruled out.

The apparent $K_{i,Ald,2}$ values given in Table 5 were calculated according to eq 20 (see section 5.4), assuming

Table 5. **Apparent $q_{max,2}$, $K_{s,Alc}$, and $K_{i,Ald,2}$ values of *E. coli* JM101 (pSPZ3) for the second reaction step determined at different inhibitor (DMB-aldehyde) concentrations[a]**

DMB-aldehyde concentration [mmol L_{aq}^{-1}]	apparent[a] $q_{max,2}$ [U (g of CDW)$^{-1}$]	apparent[a] $K_{s,Alc}$ [μmol L_{aq}^{-1}]	apparent[a] $K_{i,Ald,2}$[b] [μmol L_{aq}^{-1}]
0	93 ± 3	24 ± 3	
0.1	88 ± 4	51 ± 8	84
0.5	90 ± 2	83 ± 3	195
1	74 ± 12	124 ± 36	171

[a] The term "apparent" refers to the fact that these kinetic values were determined for whole cells and in the presence of varying inhibitor (DMB-aldehyde) concentrations. CDW: cell dry weight. [b] Apparent $K_{i,Ald,2}$ values were calculated according to eq 20, assuming competitive inhibition and normalizing $q_{max,2}$ at 93 U (g of CDW)$^{-1}$ (see section 5.4).

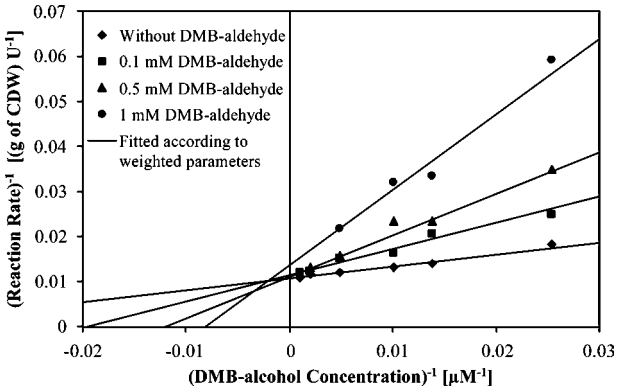

Figure 7. **Lineweaver−Burk plots for DMB-alcohol oxidation catalyzed by *E. coli* JM101 (pSPZ3) in the absence and in the presence of varying initial amounts of the product DMB-aldehyde. Whole-cell assays to determine weighted apparent $q_{max,2}$ and $K_{s,Alc}$ values were performed as described in section 5.4.**

(67) Stancik, L. M.; Stancik, D. M.; Schmidt, B.; Barnhart, D. M.; Yoncheva, Y. N.; Slonczewski, J. L. *J. Bacteriol*. **2002**, *184*, 4246−4258.

competitive inhibition and normalizing $q_{max,2}$ at 93 U (g of CDW)$^{-1}$ = 5.58 mmol (g of CDW)$^{-1}$ h^{-1}. The variance of the apparent $K_{i,Ald,2}$ with inhibitor concentration may be due to various additional factors determining the kinetics of whole-cell biocatalysts, as compared to kinetics of isolated enzymes, such as membrane permeability and cofactor availability. For the oxygenation of DMB-aldehyde to DMB-acid by *E. coli* JM101 (pSPZ3), we could not identify Michaelis−Menten-like kinetics.[24] In further analyses, we observed a sigmoid rather than hyperbolic dependence of the reaction rate on the DMB-aldehyde concentration (results not shown), suggesting allosteric effects caused by DMB-aldehyde. Such effects might also influence DMB-alcohol oxidation, thus partially overriding the inhibition by DMB-aldehyde at high DMB-aldehyde concentrations. Moreover, the kinetic analyses in aqueous single-phase systems showed that, at DMB-aldehyde concentrations above its water solubility, increasing aldehyde amounts still caused increasing DMB-acid formation rates, suggesting direct aldehyde uptake from organic-phase droplets.[24] Such interactions of DMB-aldehyde in the organic BEHP phase with the cells in the aqueous phase might explain the difference between the apparent inhibition constants determined in an aqueous single-phase system (Table 5) and the value for $K_{i,Ald,2}$ (4 μM) obtained by parameter fitting using the model for the two-liquid-phase process. Such a direct uptake of DMB-aldehyde from the BEHP phase would influence the bioconversions of DMB-aldehyde, especially its reduction to DMB-alcohol by *E. coli* dehydrogenases.

However, the experimental analysis of the kinetics of the second reaction step confirmed the inhibition by DMB-aldehyde predicted by the model. Model II for the rate equations even predicted a competitive type of inhibition, for which clear experimental evidence was found.

3.2.4. Organic−Aqueous Mass Transfer. The mass transfer coefficient for the interexchange of reactants between the aqueous and the organic phase, $(k_La)_{org/aq}$, was estimated to be around 1500 h^{-1} on laboratory scale (2 L) and 500 h^{-1} on technical scale (30 L) (see section 2). To examine the influence of $(k_La)_{org/aq}$ and of organic−aqueous mass transfer in general on the biotransformation pattern, we performed a sensitivity analysis for $(k_La)_{org/aq}$. Panel A of Figure 8 shows the simulation results for biotransformation I (2-L scale, pH 7.1), for which a $(k_La)_{org/aq}$ value of 1500 h^{-1} has been used for the simulation shown in Panel A of Figure 6. Increasing this value had only a minor impact on the biotransformation pattern, which also applies to a decrease down to 500 h^{-1}. Below a $(k_La)_{org/aq}$ value of 500 h^{-1}, the simulated DMB-aldehyde accumulation is somewhat slower and the transient DMB-alcohol accumulation higher, which is due to a lower reaction rate for the second step. The same was found for biotransformation IV on a 30-L scale including pH shifts (Figure 8 B). Here, a $(k_La)_{org/aq}$ of 500 h^{-1} has been used for the simulation shown in Panel D of Figure 6. The relatively low sensitivity of the first oxidation step to $(k_La)_{org/aq}$ can be ascribed to the contribution of direct pseudocumene uptake from the organic phase to the total substrate uptake. It cannot be excluded that such direct uptake also occurs for DMB-alcohol and DMB-aldehyde (see above). However, for these reactants the contribution of direct uptake would be low in the biotransformation system under investigation since their aqueous concentrations are considerably higher as compared to those of pseudocumene. This and the inhibition of their oxygenation by other reactants, which in turn may also be influenced by direct interactions between cells and solvent droplets, complicate the identification of a potential direct uptake from the organic phase.

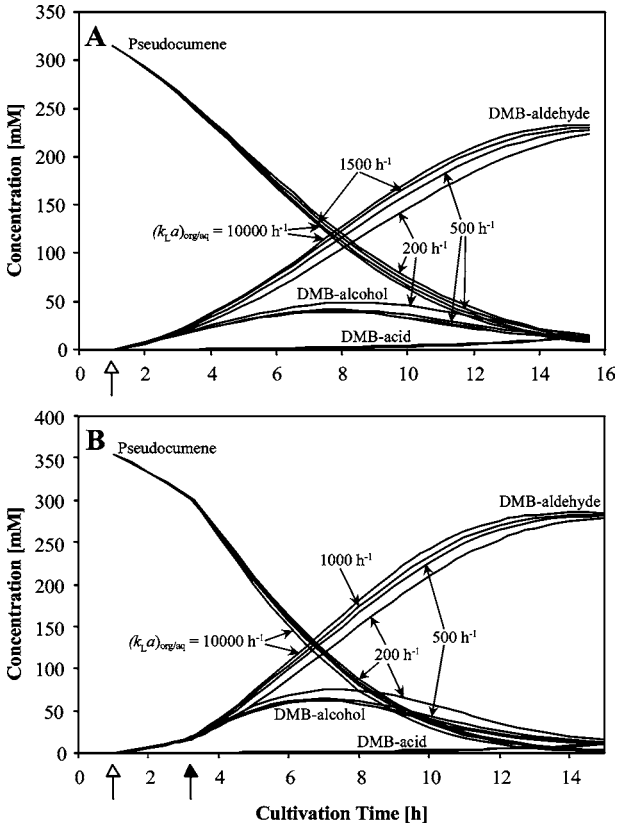

Figure 8. **Sensitivity analyses for the organic−aqueous mass transfer coefficient $(k_La)_{org/aq}$. The effect of varying the $(k_La)_{org/aq}$ between 200 and 10000 h^{-1} on the course of substrate and product concentrations is shown for biotransformations I (A) and IV (B). Model II for the rate equations including metabolic inhibition, was used for the simulation of the bioconversion. Open arrows indicate organic phase addition. The closed arrow in panel B indicates the change of the modeling parameters as a consequence of the pH shifts in biotransformation IV. Growth and bioconversion parameters used for the simulations are shown in Tables 1 and 2, respectively.**

Pereira et al. also used a modeling approach to describe the interfacial mode of activity of hydroxynitrile lyase in a diisopropyl ether/aqueous buffer two-liquid-phase system.[68] This system was reported to show a linear dependence of the reaction rate on interfacial area and enzyme activity exclusively at the interface.[69] The model proposed a two-layer adsorption mechanism at the interface with a first layer consisting of unfolded enzymes with lower activity and a second layer consisting of native enzymes.[68] Gerrits et al. exploited mass transfer limitation in a similar system with

(68) Pereira, L. G. C.; Hickel, A.; Radke, C. J.; Blanch, H. W. *Biotechnol. Bioeng.* **2002**, *78*, 595−605.
(69) Hickel, A.; Radke, C. J.; Blanch, H. W. *Biotechnol. Bioeng.* **1999**, *65*, 425−436.

methyl *tert*-butyl ether as organic solvent to enhance the enantiomeric excess in the hydroxynitrile lyase-based synthesis of chiral cyanohydrins.[70,71] However, such a process for the production of (*R*)-mandelonitrile from benzaldehyde and hydrogen cyanide was consistently modeled without considering enzyme activity at the interface but assuming the reaction to occur in the bulk of the aqueous phase and by modeling substrate mass transfer from the organic to the aqueous phase.[39,72] A comparative evaluation of the mass transfer model and the adsorbed enzyme model showed that the two mechanisms have qualitatively similar consequences and suggested that both models may be valid simultaneously.[73] Further developed versions of the mass transfer model, which is similar to the model developed in this study, facilitated reaction temperature optimization[38] and allowed comparisons of batch, fed-batch, and continuous modes of operation.[74] Modeling indicated that continuous operation is not feasible and that the choice between batch and fed-batch operation depends on reactor and enzyme costs. It also facilitated the development of a process for the production of (*R*)-4-hydroxymandelonitrile from 4-hydroxybenzaldehyde and hydrogen cyanide.[75] Cruickshank et al.[37] modeled phenol degradation by *P. putida* in a 2-undecanone-based aqueous−organic two-liquid-phase system and identified oxygen mass transfer as the main factor restricting the amount of phenol degradation over time, whereas phenol mass transfer was not limiting. This process model was used to optimize the phenol feeding strategy and included a cell entrainment factor to simulate the loss of active cells to the organic phase and due to biofilm formation in the form of foam and wall growth.[76]

In the process investigated in this study, we observed no significant cell loss, no cell adsorption to the interphase (results not shown), and no significant dependence of the specific reaction rates on power input (scale).[26] The developed model considers the reactions to occur in the bulk of the aqueous phase and additionally assumes direct pseudocumene uptake from the organic phase via collisions of cells and solvent droplets. The poor impact of the $(k_La)_{org/aq}$ on overall process performance indicates that, also on a technical scale, substrate−cell transfer is efficient and that, at the actual state of the process, other factors primarily affect the productivity of the whole-cell-based two-liquid-phase biotransformation of pseudocumene to DMB-aldehyde. Such limiting factors may include intrinsic enzyme activity, oxygen supply, and as indicated in this study, the cofactor regeneration capacity, which is linked to cell viability. Studies on octane mass transfer in two-liquid-phase cultures of *P. putida* GPo1 growing on octane contained in hexadecene as organic carrier solvent suggested that high solvent−cell transfer rates may also be achievable in biocatalytic two-liquid-phase processes using recombinant strains for the production of a specific metabolic pathway intermediate, which is not further degraded.[40,77] Together with the effective production of (*S*)-styrene oxide on pilot-scale by *E. coli* containing a recombinant styrene monooxygenase,[78] the efficient solvent−cell transfer attained for DMB-aldehyde production confirms this assessment.

4. Conclusions

A process model has been developed to describe the multistep bioconversion of pseudocumene to DMB-aldehyde in a BEHP-based two-liquid-phase system catalyzed by recombinant *E. coli* containing XMO and growing in fed-batch mode. The correlation between simulation and experimental results of biotransformations at varying conditions was high with respect to the course of the substrate and product concentrations. Simulation of cell growth meets the main goal to predict the biocatalyst concentration. The variation of the growth parameters during biotransformation is suboptimal but allows the conclusion that bioconversion and pH have an impact on cell growth.

A comparison of the kinetics of the multistep oxygenation of pseudocumene in the aqueous single-phase system with the kinetics in the two-liquid-phase system and process simulation indicated the occurrence of pseudocumene uptake directly from the organic phase. An increase of the pH from 7.1 to 7.4 has been found to increase biocatalyst activity at the expense of cell growth[26] pointing to a pH-influenced competition for NADH between XMO and the respiratory chain. The introduction of a pH-dependent feedback inhibition of the NADH-consuming bioconversions as a modeling tool allowed good simulations of the multistep biooxidation of pseudocumene in experiments performed at varying pH, scale, and initial substrate concentration. This consistent process simulation supported the assumed intracellular NADH shortage and the consequential pH-influenced competition for NADH. Furthermore, modeling and simulation indicated competitive inhibition of the second oxidation step by DMB-aldehyde, which could be confirmed experimentally. A sensitivity analysis for $(k_La)_{org/aq}$ indicated that the organic−aqueous mass transfer does not affect the overall productivity of the process under the conditions applied and emphasized the efficient substrate−cell transfer in the BEHP-based two-liquid-phase system. These results indicate that biological energy shortage may be a key limiting factor in biooxidation processes based on growing cells.

The described model represents a first step towards the complete modeling of this biotransformation process. Ongoing research concentrates on the investigation of the interrelationship between bioconversion, cell growth, energy metabolism, and acetic acid formation and thus is supposed to enable a more detailed modeling of bioconversion and especially cell growth. The successful simulations illustrate

(70) Gerrits, J. G.; Marcus, J.; Birikaki, L.; van der Gen, A. *Tetrahedron: Asymmetry* **2001**, *12*, 971−974.
(71) Gerrits, P. J.; Willeman, W. F.; Straathof, A. J. J.; Heijnen, J. J.; Brussee, J.; van der Gen, A. *J. Mol. Catal.* B: *Enzym.* **2001**, *15*, 111−121.
(72) Willeman, W. F.; Hanefeld, U.; Straathof, A. J. J.; Heijnen, J. J. *Enzyme Microb. Technol.* **2000**, *27*, 423−433.
(73) Straathof, A. J. J. *Biotechnol. Bioeng.* **2003**, *83*, 371−375.
(74) Willeman, W. F.; Straathof, A. J. J.; Heijnen, J. J. *Bioprocess Biosyst. Eng.* **2002**, *24*, 281−287.
(75) Willeman, W. F.; Neuhofer, R.; Wirth, I.; Pöchlauer, P.; Straathof, A. J. J.; Heijnen, J. J. *Biotechnol. Bioeng.* **2002**, *79*, 154−164.
(76) Collins, L. D.; Daugulis, A. J. *Biotechnol. Bioeng.* **1997**, *55*, 155−162.
(77) Schmid, A.; Kollmer, A.; Mathys, R. G.; Witholt, B. *Extremophiles* **1998**, *2*, 249−256.
(78) Panke, S.; Held, M.; Wubbolts, M. G.; Witholt, B.; Schmid, A. *Biotechnol. Bioeng.* **2002**, *80*, 33−41.

the potential of the model for future characterization and optimization of the present process and especially analogous processes using the same catalyst and concept for the production of different oxidation products. The model and results of this study will also provide valuable theoretical background for other two-liquid-phase biooxidation processes based on growing cells.

5. Experimental Section

5.1. Bacterial Strain, Plasmid, and Chemicals. *E. coli* JM101 (*supE thi* Δ(*lac-proAB*) F′[*traD*36 *proAB*$^+$ lacI^q *lacZ*ΔM15]),[79] an *E. coli* K-12 derivative, was used as recombinant host strain. As expression vector, we used the pBR322-derived plasmid pSPZ3 containing the XMO genes *xylMA* under the control of the *alk* regulatory system of *P. putida* GPo1.[22] The High Pure Plasmid Isolation Kit of Roche Diagnostics (Mannheim, Germany) was used to prepare plasmid DNA following the supplier's protocol. Chemicals were obtained from Fluka (Buchs, Switzerland) (pseudocumene, ∼99%; DMB-acid, ∼97%; BEHP, 97%), Aldrich (Buchs, Switzerland) (DMB-alcohol, 99%), Lancaster (Muehlheim, Germany) (DMB-aldehyde, 97%), and Acros Organics (Geel, Belgium) (*n*-octane, >98.5%).

5.2. Media and Growth Conditions. Bacteria were either grown in Luria-Bertani (LB) broth (Difco, Detroit, MI) or the minimal media MS or RB.[25] In all cases, the growth temperature was 30°C. Complex media contained 50 mg L^{-1} kanamycin and 10 g L^{-1} glucose to avoid indigo formation.[22] Minimal media contained per liter 5 or 7 g of glucose, 10 mg of thiamine, 50 mg of kanamycin, and 1 mL of trace element solution US^{Fe}, of which the composition is described elsewhere.[24,25] Solid media contained 1.5% (wt/vol) agar. Shaking flask cultures were routinely incubated on horizontal shakers at 200 rpm. The setup and the procedure of the two-liquid-phase biotransformations at different scales and pH as well as the process analytics have been described in earlier publications.[24−26]

5.3. Analysis of Metabolites. The quantitative analysis of *n*-octane, pseudocumene, 3,4-dimethylbenzyl alcohol, 3,4-dimethylbenzaldehyde, and 3,4-dimethylbenzoic acid was performed via gas chromatography (GC) and high-performance liquid chromatography (HPLC) as described elsewhere.[23,24]

5.4. Whole-Cell Assays. Whole-cell assays to study the kinetics and pH dependency of the three monooxygenation steps catalyzed by XMO included cell growth, induction, resting cell biotransformations at a 1-mL scale, and sample preparation for GC and HPLC analysis and were performed as described before,[23] including induction by 0.1% (vol/vol) *n*-octane and cell concentrations in the resting cell biotransformations between 0.1 and 1.3 g of cell dry weight (CDW) per liter.

In experiments to investigate the pH dependency of the specific activities of *E. coli* JM101 (pSPZ3), samples of cells were incubated for 5 min with 0.5 mM of pseudocumene, DMB-alcohol, or DMB-aldehyde in 50 mM potassium phosphate buffer at different pH, 30°C, and a cell concentration of about 0.5 (g of CDW) L^{-1}. The assays were carried out twice independently. Initial specific activities were calculated as average activities based on the sum of all products formed in 5 min of reaction. One unit (U) is defined as the activity that forms 1 μmol of total products in 1 min. Specific activity was expressed as activity per g of CDW [U (g of CDW)$^{-1}$].

The kinetic parameters $q_{max,2back}$ and $K_{m,Ald,back}$ ($=K_{s,Ald,back}$) for the dehydrogenase-type DMB-aldehyde reduction to DMB-alcohol catalyzed by *E. coli* JM101 without plasmid were determined in reactions carried out for 5 and 10 min with DMB-aldehyde concentrations ranging from 0.04 to 4 mM and a biocatalyst concentration of 1.28 (g of CDW) L^{-1}. The assays were carried out twice independently and specific activities were calculated based on the amount of DMB-alcohol formed using the program Leonora designed to analyze enzyme kinetic data and described by Cornish-Bowden.[80]

The apparent maximal reaction velocities, $q_{max,2}$, and substrate uptake constants, $K_{s,Alc}$, for DMB-alcohol oxidation at different inhibiting DMB-aldehyde concentrations (0, 0.1, 0.5, and 1 mM) catalyzed by *E. coli* JM101 (pSPZ3) were determined in duplicate reactions carried out for 5 min with DMB-alcohol concentrations ranging from 0.04 to 1 mM and a biocatalyst concentration of 0.097 (g of CDW) L^{-1}. Such a low biocatalyst concentration was chosen to minimize the formation of a product mixture and to avoid significant substrate depletion. Specific activities were calculated on the basis of the amount of products formed. Apparent $q_{max,2}$ and $K_{s,Alc}$ values were calculated using the program Leonora. The term "apparent" refers to the fact that these kinetic values were determined for whole cells and in the presence of varying inhibitor (DMB-aldehyde) concentrations. As in the modeling, the substrate uptake constants K_s were assumed to be actually K_m values. Apparent inhibition constants, $K_{i,Ald,2}$, were calculated according to the following correlation for competitive inhibition:

$$K^*_{m,Alc} = K_{m,Alc} \cdot \left(1 + \frac{C^{aq}_{Ald}}{K_{i,Ald,2}}\right) \qquad [\text{mmol } L_{aq}{}^{-1}] \qquad (20)$$

In eq 20, $K^*_{m,Alc}$ and $K_{m,Alc}$ represent the apparent $K_{s,Alc}$ values at the DMB-aldehyde concentrations C^{aq}_{Ald} and in the absence of DMB-aldehyde, respectively.

5.5. Process Simulation. The system of mathematical equations was programmed within Matlab version 6.1 (The Mathworks, Natick, MA), using the Simulink Block Library version 3.

Acknowledgment

We thank Dr. F. Hollmann and Dr. K. Otto for critical reading of the manuscript. Financial support of the BASF Corporation (Ludwigshafen, Germany) is gratefully acknowledged.

(79) Messing, J. *Recomb. DNA Technol. Bull.* **1979**, *2*, 43−49.

(80) Cornish-Bowden, A. *Analysis of Enzyme Kinetic Data*; Oxford University Press: New York, 1995.

GLOSSARY

C_a^{aq}	concentration in aqueous phase [mmol L_{aq}^{-1}]
C_a^{org}	concentration in organic phase [mmol L_{org}^{-1}]
$C_{a,0}^{org}$	initial concentration in organic phase [mmol L_{org}^{-1}]
C_b^{aq}	inhibitor concentration in aqueous phase [mmol L_{aq}^{-1}]
C_{Glc}^{aq}	glucose concentration in aqueous phase [g L_{aq}^{-1}]
$C_{Glc,0}^{aq}$	initial glucose concentration in aqueous phase [g L_{aq}^{-1}]
C_{Glc}^{feed}	glucose concentration in feeding solution [g L_{feed}^{-1}]
$C_{O_2}^{aq}$	oxygen concentration in aqueous phase [mmol L_{aq}^{-1}]
$C_{O_2,0}^{aq} = C_{O_2}^*$	aqueous oxygen concentration in equilibrium [mmol L_{aq}^{-1}]
C_X	biomass concentration [(g of CDW) L_{aq}^{-1} or mCmol L_{aq}^{-1}]
$C_{X,0}$	initial biomass concentration [(g of CDW) L_{aq}^{-1}]
F	aqueous glucose feed flow [L_{feed} h^{-1}]
F_{sample}	sample flow [L h^{-1}]
$K_{m,a}(= K_{s,a})$	Michaelis (substrate uptake) constant for oxygenation of compound a [mmol L_{aq}^{-1}]
$K_{m,Ps,org}$	Michaelis constant for pseudocumene uptake from organic phase [mmol L_{org}^{-1}]
$K_{m,Ald,back}$	Michaelis constant for back reaction of DMB-aldehyde to DMB-alcohol [mmol L_{aq}^{-1}]
$K_{m,Alc}^*$	Michaelis constant for DMB-alcohol oxygenation in the presence of inhibiting DMB-aldehyde [mmol L_{aq}^{-1}]
$K_{i,b,n}$	inhibition constant for compound b and reaction n [mmol L_{aq}^{-1}]
$K_{p,a}$	partition coefficient for compound a [L_{aq} L_{org}^{-1}]
$K_{s,Glc}$	saturation (Monod) constant for glucose [g L_{aq}^{-1}]
K_{s,O_2}	saturation (Monod) constant for oxygen [mmol L_{aq}^{-1}]
k_{evap}	evaporation rate constant for pseudocumene [h^{-1}]
$(k_La)_{org/aq}$	organic−aqueous mass transfer coefficient [h^{-1}]
$(k_La)_{O_2}$	gas−aqueous mass transfer coefficient for oxygen [h^{-1}]
M_i	metabolic inhibition coefficient [mmol (g of CDW)$^{-1}$ h^{-1}]
m_{Glc}	maintenance coefficient for glucose [g (g of CDW)$^{-1}$ h^{-1} or mCmol mCmol^{-1} h^{-1}]
m_{O_2}	maintenance coefficient for oxygen [mmol (mCmol biomass)$^{-1}$ h^{-1}]
$q_{max,n}$	maximal rate for reaction n [mmol (g of CDW)$^{-1}$ h^{-1}]
r_n	reaction rate for step n [mmol L_{aq}^{-1} h^{-1}]
$r_{P,NADH}$	total NADH coupled bioconversion rate [mmol L_{aq}^{-1} h^{-1}]
r_{Glc}	glucose consumption rate [g L_{aq}^{-1} h^{-1}]
r_{O_2}	oxygen consumption rate [mmol L_{aq}^{-1} h^{-1}]
r_X	biomass formation rate [(g of CDW) L_{aq}^{-1} h^{-1}]
t	time [h]
t_0	start of fed-batch cultivation [h]
t_{org}	time of organic phase addition [h]
V^{aq}	aqueous phase volume [L_{aq}]
V^{org}	organic phase volume [L_{org}]
V_0^{aq}	aqueous phase volume at t_0 [L_{aq}]
V_0^{org}	organic phase volume at t_{org} [L_{org}]
$Y_{P/Glc}^{max}$	maximal yield of reaction steps on glucose [mmol mCmol^{-1}]
Y_{P/O_2}^{max}	maximal yield of reaction steps on oxygen [mmol mmol^{-1}]
$Y_{X/Glc}^{max}$	maximal yield of biomass on glucose [(g of CDW) g^{-1} or mCmol mCmol^{-1}]
Y_{X/O_2}^{max}	maximal yield of biomass on oxygen [mCmol mmol^{-1}]
$Y_{O_2/Glc}$	glucose-dependent oxygen demand [mmol mCmol^{-1}]
φ_{evap}	pseudocumene evaporation rate [mmol L_{org}^{-1} h^{-1}]
φ_a	organic−aqueous transfer rate of compound a [mmol L_{aq}^{-1} h^{-1}]
φ_{O_2}	oxygen transfer rate [mmol L_{aq}^{-1} h^{-1}]
μ_{max}	maximum specific growth rate [h^{-1}]

Compounds a and b (inhibiting):

Ps	pseudocumene
Alc	3,4-dimethylbenzyl alcohol
Ald	3,4-dimethylbenzaldehyde
Acid	3,4-dimethylbenzoic acid

Reaction step n:

1	Ps → Alc
1org	Ps → Alc (Ps uptake from organic phase)
2	Alc → Ald
2back	Ald → Alc
3	Ald → Acid

Received for review February 2, 2006.

OP060028G